ANTIOXIDANTS & REDOX SIGNALING
Volume 11, Number 4, 2009

DOI: 10.1089/ars.2008.2203

Forum Original Research Communication

Role of Nox4 and Nox2 in Hyperoxia-Induced Reactive Oxygen Species Generation and Migration of Human Lung Endothelial Cells

Srikanth Pendyala,[1] Irina A Gorshkova,[1] Peter V. Usatyuk,[1] Donghong He,[1] Arjun Pennathur,[2] J. David Lambeth,[3] Victor J. Thannickal,[4] and Viswanathan Natarajan[1]

Abstract

In vascular endothelium, the major research focus has been on reactive oxygen species (ROS) derived from Nox2. The role of Nox4 in endothelial signal transduction, ROS production, and cytoskeletal reorganization is not well defined. In this study, we show that human pulmonary artery endothelial cells (HPAECs) and human lung microvascular endothelial cells (HLMVECs) express higher levels of Nox4 and $p22^{phox}$ compared to Nox1, Nox2, Nox3, or Nox5. Immunofluorescence microscopy and Western blot analysis revealed that Nox4 and $p22^{phox}$, but not Nox2 or $p47^{phox}$, are localized in nuclei of HPAECs. Further, knockdown of Nox4 with siRNA decreased Nox4 nuclear expression significantly. Exposure of HPAECs to hyperoxia (3–24 h) enhanced mRNA and protein expression of Nox4, and Nox4 siRNA decreased hyperoxia-induced ROS production. Interestingly, Nox4 or Nox2 knockdown with siRNA upregulated the mRNA and protein expression of the other, suggesting activation of compensatory mechanisms. A similar upregulation of Nox4 mRNA was observed in Nox2 $^{-/-}$ ko mice. Downregulation of Nox4, or pretreatment with *N*-acetylcysteine, attenuated hyperoxia-induced cell migration and capillary tube formation, suggesting that ROS generated by Nox4 regulate endothelial cell motility. These results indicate that Nox4 and Nox2 play a physiological role in hyperoxia-induced ROS production and migration of ECs. *Antioxid. Redox Signal*. 11, 747–764.

Introduction

Reactive oxygen species (ROS) are conventionally viewed as toxic byproducts of cellular metabolism. On the other hand, organisms possess enzymatic systems that generate ROS under physiological conditions (36). Among the enzymatic systems that are well characterized is the superoxide-producing NADPH oxidase in mammalian phagocytes that play crucial roles in host defense against microbial infection (2, 3). The catalytic core of the phagocytic NADPH oxidase is the membrane-integrated flavocytochrome b_{558}, comprising the two subunits $p22^{phox}$ and Nox2 ($gp91^{phox}$); the latter contains a complete electron-transferring apparatus from NADPH to molecular oxygen with binding sites for heme, FAD, and NADPH (5, 8, 34). The phagocytic NADPH oxidase, dormant in resting cells, becomes activated during phagocytosis to generate superoxide ($O_2^{\cdot-}$). The activation requires the two specialized cytosolic proteins, $p47^{phox}$ and $p67^{phox}$, and the small GTPase Rac2, all of which are translocated upon cell stimulation to the membrane to interact with and activate the flavocytochrome (23). Such a strict regulation of the phagocyte oxidase activity is critical, as uncontrolled production of high concentrations of ROS is injurious not only to phagocytes themselves but also to their surrounding tissues. This may further amplify the inflammatory response and perpetuate tissue damage.

Although Nox2 is a critical component of the phagocytic NADPH oxidase, the role of Nox2 and Nox2-generated ROS in vascular cells remains somewhat controversial and may

[1]Department of Medicine, The University of Chicago, Chicago, Illinois.
[2]Department of Thoracic Surgery, University of Pittsburgh, Pittsburgh, Pennsylvania.
[3]Department of Pathology, Emory University, Atlanta, Georgia.
[4]Department of Internal Medicine, University of Michigan, Ann Arbor, Michigan.

depend on specific cell types within the vessel wall (6, 38). For example, expression of Nox2 has been reported in arteriolar smooth muscle cells (SMC), but not in aortic SMC. In human pulmonary artery smooth muscle cells (PASMCs), human urotensin II-mediated activation of NADPH oxidase was abrogated by $p22^{phox}$ or Nox4 antisense oligonucleotides, and depletion of Nox4 or $p22^{phox}$ blocked urotensin-II, but not S1P, mediated proliferation of PASMCs (9). These data suggest potential involvement of Nox4 or $p22^{phox}$ in mitogenesis. Further, in 3T3-L1 adipocytes, Nox4 but not Nox2, appears to be the major mediator of insulin-induced ROS production associated with oxidative inhibition of PTP1B activity (25). A role for Nox4 and JNK signaling has been implicated in 7-ketocholesterol-mediated NADPH oxidase activation and overproduction of ROS in human aortic smooth muscle cells (28).

ROS, including hydrogen peroxide (H_2O_2) and $O_2^{\cdot -}$, function as signaling molecules in vascular endothelial and smooth muscle cells (24). We have demonstrated that hyperoxia activated human lung endothelial cell NADPH oxidase with enhanced production of ROS including $O_2^{\cdot -}$(27). Further, a role for Src kinase (7) and cortactin (37) in hyperoxia-induced activation of $p47^{phox}$ was demonstrated in human pulmonary artery endothelial cells (HPAECs). Recent studies have shown that all the Nox and phox components of phagocytic oxidase are also present in vascular cells (6); however, the effect of hyperoxia on the expression of Nox and phox proteins and their role in hyperoxia-induced $ROS/O_2^{\cdot -}$ are yet to be fully defined. In the present study, we evaluated the expression profiles of Nox and phox family of proteins under normoxia and hyperoxia and the role of Nox4 and Nox2 in hyperoxia-induced ROS production. Our results demonstrate that: (a) mRNA expressions of Nox4 and $p22^{phox}$, as determined by real-time PCR, are very high compared to other Nox and phox proteins; (b) exposure of HPAECs to hyperoxia further enhanced the mRNA expressions of Nox1, Nox2, Nox4, and $p22^{phox}$;; (c) the protein expression of Nox2, Nox4, and $p22^{phox}$, were also increased by hyperoxia; (d) under normoxia, Nox4 in pulmonary artery endothelial cells is predominantly expressed in the nucleus as compared to Nox2 and $p22^{phox}$, which are localized in the cytoplasmic compartment; (e) Nox2 and Nox4 knockdown with specific siRNAs attenuated hyperoxia-induced ROS generation; (f) Nox4 siRNA upregulated mRNA and protein expression of Nox2, while Nox2 siRNA increased the expression of Nox4; (g) deletion of Nox2 gene in mice upregulated expression of Nox4 and $Nox2^{-/-}$ mice exhibited ROS accumulation in bronchoalveolar lavage (BAL) fluids; and (h) exposure of $Nox2^{-/-}$ mice to hyperoxia did not further increase Nox4 mRNA levels.

Materials and Methods

Materials

HPAECs, human lung microvascular endothelial cells (HLMVECs), EBM-2 basal media, and Bullet kit were obtained from Clonetics (San Diego, CA). Phosphate-buffered saline (PBS) was from Biofluids Inc. (Rockville, MD). Ampicillin, fetal bovine serum (FBS), trypsin, $MgCl_2$, EGTA, Tris-HCl, Triton X-100, sodium orthovanadate, aprotinin, Tween 20, ferricytochrome *c*, polyethylene glycol-(PEG) conjugated superoxide dismutase (SOD), and H_2O_2 (30%), were all obtained from Sigma (St. Louis, MO). Dihydroethidium (hydroethidine), 6-carboxy-2′,7′-dichlorodihydrofluorescein diacetate, di (acetoxymethyl ester) (DCFDA), were purchased from Molecular Probes (Eugene, OR). ECL kit was from Amersham Biosciences, Piscataway, NJ. SMART Pool® small interfering RNA duplex oligonucleotides targeting $p47^{phox}$ were purchased from Dharmacon, Inc. (Lafayette, CO). Nox4 siRNA was purchased from Ambion (Austin, TX), and Nox2 siRNA were purchased from Santa Cruz Biotechnology (Santa Cruz, CA). Polyclonal antibodies to Nox4, Nox2, and $p22^{phox}$ were procured from Santa Cruz Biotechnology. Calreticulin was purchased from Abcam. (Cambridge, MA). Nox4 antibody for Immunocytochemistry was provided by Dr. David Lambeth (Emory University, Atlanta, GA).

Endothelial cell culture

HPAECs and HLMVECs, passages between 5 and 8, were grown in EGM-2 complete media with 10% FBS, 100 Units/ml penicillin, and streptomycin in a 37°C incubator under 5% CO_2, 95% air atmosphere, and grown to contact-inhibited monolayers with typical cobblestone morphology as described previously (7, 27). Cells from T-75 flasks were detached with 0.05% trypsin, resuspended in fresh complete medium, and cultured in 35- or 60-mm dishes or on glass coverslips for immunofluorescence studies.

Exposure of cells to hyperoxia

HPAECs (~90% confluence) in complete EGM-2 medium were placed in a humidity-controlled airtight modulator incubator chamber (Billups-Rothenberg, Del Mar, CA), flushed continuously with 95% O_2, 5% CO_2 for 30 min until the oxygen level inside the chamber reached ~95%. HPAECs were then placed in a cell culture incubator at 37°C for the desired lengths of time (3–72 h). The concentration of O_2 inside the chamber was monitored with a digital oxygen monitor. The buffering capacity of the cell culture medium did not change significantly during the period of hyperoxic exposure and was maintained at a pH ~7.4. In some experiments, cells were pretreated with PEG-conjugated SOD at 400 Units/mL for 1 h prior to addition of dihydroethidium or DCFDA and exposure to hyperoxia (3 h).

RNA isolation and real time RT-PCR

Total RNA was isolated from HPAECs grown on 35-mm dishes using TRIzol® reagent (Invitrogen, Carlsbad, CA), according to the manufacturer's instruction. iQ SYBR Green Supermix was used to do the real time using iCycler by Biorad (Hercules, CA). 18S rRNA (sense, 5′-GTAACCCGTTGAACCCCATT-3′, and antisense, 5′-CCATCCAATCGGTAGTAGCG-3′) was used as a housekeeping gene to normalize expression. The reaction mixture consisted of 0.3 μg of total RNA (target gene) or 0.03 μg of total RNA (18 S rRNA), 12.5 μl of iQ SYBR Green, 2 μl of cDNA, 1.5 μM target primers, or 1 μM 18 S rRNA primers, in a total volume of 25 μl. For all samples, reverse transcription was carried out at 25°C for 5 min, followed by cycling to 42°C for 30 min, and 85°C for 5 min with iScript cDNA synthesis kit. Amplicon expression in each sample was normalized to its 18 S rRNA content. The relative abundance of target mRNA in each sample was calculated as 2 raised to the negative of its threshold cycle value times 10^6 after being

normalized to the abundance of its corresponding 18 S rRNA,$(2^{-(\text{primer Threshold Cycle})}/2^{-(18\text{ S Threshold Cycle})} \times 10^6)$. All primers were designed by inspection of the genes of interest and were designed using Beacon Designer 2.1 software (Palo Alto, CA). Negative controls, consisting of reaction mixtures containing all components except target RNA, were included with each of the RT-PCR runs. To verify that amplified products were derived from mRNA and did not represent genomic DNA contamination, representative PCR mixtures for each gene were run in the absence of the RT enzyme after first being cycled to 95°C for 15 min. In the absence of reverse transcription, no PCR products were observed.

Preparation of nuclear extracts

Nuclear extracts were prepared from HPAECs according to the manufacturer's instructions (Active Motif North America, Carlsbad, CA). Briefly, cells were collected by scraping in ice-cold PBS with phosphatase inhibitors and pelleted by centrifuging at 1,000 *g* for 5 min. The pellet was resuspended in 500 μl of 1X hypotonic buffer and incubated on ice for 15 min, followed by addition of 25 μl of detergent and high speed vortexing for 30 s, following the manufacturer's recommendation. The suspension was centrifuged at 14,000 *g* for 20 min in a microcentrifuge at 4°C; the nuclear pellet was resuspended in 50 μl of lysis buffer A and incubated on ice for 15 min. This suspension was centrifuged for 10 min at 14,000 *g* in a microcentrifuge, and the supernatant (nuclear extract) was aliquoted and stored at −80°C for further analysis. Protein in the nuclear extract was quantified by BCA protein assay.

Determination of hyperoxia-induced production of $O_2^{\cdot -}$, and total ROS

Two methods were used to measure total ROS or $O_2^{\cdot -}$ by spectrofluorimetry or fluorescence microscopy. Hyperoxia-induced $O_2^{\cdot -}$ release by HPAECs was measured by hydroethidine fluorescence as described (7, 27). Total ROS production in HPAECs exposed to either normoxia or hyperoxia was determined by the DCFDA fluorescence method (16). Briefly, HPAECs (~90% confluent in 35-mm dishes) were loaded with 10 μM DCFDA in EGM-2 basal medium and incubated at 37°C for 30 min. Fluorescence of oxidized DCFDA in cell lysates, an index of formation of ROS, was measured with an Aminco Bowman series 2 spectrofluorimeter (Waltham, MA) using excitation and emission set at 490 and 530 nm, respectively, with appropriate blanks. Hyperoxia-induced ROS formation in cells was also quantified by fluorescence microscopy. HPAECs (~90% confluent) in 35-mm dishes were loaded with DCFDA (10 μM) in EBM-2 basal medium for 30 min at 37°C in a 95% air, 5% CO_2 environment. After 30 min of loading, the medium containing DCFDA was aspirated; cells were rinsed once with EGM-2 complete medium; cells were preincubated with agents for the indicated time periods, followed by exposure to either normoxia (95% air, 5% CO_2) or hyperoxia (95% O_2, 5%CO_2) for 3–72 h. At the end of the incubation, cells were washed twice with PBS at room temperature and were examined under a Nikon Eclipse TE 2000-S fluorescence microscope with Hamamatsu digital CCD camera (Bridgewater, NJ) using a 20X objective lens and MetaVue software (Universal Imaging Corp., PA). For measuring superoxide $O_2^{\cdot -}$ in the nucleus of HPAECs, DHE (dihydroethidium, Invitrogen, Inc.) was loaded 30 min prior to hyperoxia exposure of cells for 3h. Images were taken with Nikon Eclipse Microscope at 60X.

Determination of H_2O_2 by Amplex Red assay

H_2O_2 formation in the medium or nuclear fraction was determined by fluorescence method using an Amplex Red Hydrogen Peroxide Assay kit (Molecular Probes). HPAECs were transfected with scrambled or Nox4 siRNA for 48 h, further, nuclear fractions were isolated with Nuclei EZ Prep Nuclei Isolation Kit (Sigma). These prepared nuclear fractions were exposed to normoxia (95% air–5% CO_2) or hyperoxia (95% O_2–5% CO_2) for 3 h in 1.0 ml of phenol red-free medium (GIBCO-BRL medium 199). At the end of incubation, the medium was collected and centrifuged at 4,000 *g* for 5 min, and fluorescence of the medium was measured on an Aminco Bowman series 2 spectrofluorimeter with excitation and emission set at 560 and 590 nm, respectively, using appropriate blanks and expressed as percentage of normoxic controls.

Immunofluorescence microscopy

HPAECs grown on coverslips to ~95% confluence in EGM-2 complete medium as indicated, followed by exposure to either normoxia or hyperoxia for 3 h. Coverslips were rinsed with phosphate-buffered saline and treated with 3.7% formaldehyde in phosphate-buffered saline at room temperature for 20 min. After washing with phosphate-buffered saline, coverslips were incubated in blocking buffer [1% bovine serum albumin in tris-buffered saline tween-20 (TBST)] for 1 h. Cells were subjected to immunostaining with total Nox4 antibody or Nox2 antibody or $p22^{phox}$ antibody (1: 200 dilution) for 1 h and washed three times with TBST, followed by staining with Alexa Fluor 488 (1:200 dilution in blocking buffer) for 1 h. After washing at least three times with TBST, the coverslips were mounted using commercial mounting medium (Kirkegaard and Perry laboratories, Gaithersburg, MD) and were examined by immunofluorescence microscopy with Hamamatsu digital camera using a 60X oil immersion objective and MetaVue software.

Immunohistochemistry

The 4-mm sections from paraffin-embedded tissues were mounted on poly-L-lysine-coated slides. After pretreatment of the sections, they were incubated with rabbit polyclonal anti-Nox2 or anti-Nox4 antibody diluted at 1:200 in a moist chamber overnight at 4°C. After washing in 0.01 *M* PBS, the sections were incubated for 30 min at room temperature with biotinylated goat anti-rabbit immunoglobulin antibody. Then, peroxidase-conjugated streptavidin (Vector Laboratories, Burlingame, CA) was applied. After washing out the excess complex, the localization of immunoreactive complexes was visualized after incubation of the sections for 5–10 min in 50 m*M* Tris–HCl (pH 7.6) containing 0.02% (wt/vol) 3,39-diaminobenzidine tetrahydrochloride and 0.03% (wt/vol) H_2O_2. Normal rabbit pre-immune serum was applied onto slides in each staining as a control.

Preparation of cell lysates and Western blot analysis

HPAECs grown on 100-mm dishes (~90% confluence) were rinsed twice with ice-cold phosphate-buffered saline

and lysed in 100 μl of modified lysis buffer (50 m*M* Tris-HCl, pH 7.4, 150 m*M* NaCl, 0.25% sodium deoxycholate, 1 m*M* EDTA, 1 m*M* phenylmethylsulfonyl fluoride, 1 m*M* Na_3VO_4, 1 m*M* NaF, 10 μg/ml aprotinin, 10 μg/ml leupeptin, and 1 μg/ml pepstatin), sonicated on ice with a probe sonicator (three times for 15 s), centrifuged at 5,000 *g* in a microcentrifuge (4°C for 5 min), and protein concentrations of the supernatants were determined using a Pierce protein assay kit. The supernatants, adjusted to 1 mg of protein/ml (cell lysates) were denatured by boiling in SDS sample buffer for 5 min, and samples were separated on 10% SDS-polyacrylamide gels and analyzed by Western blotting. Nox4 antibody was used at 1:1,000 dilution while Nox2 and $p22^{phox}$ antibodies were used at 1:2,000 dilutions. Protein bands were transferred overnight (24 V, 4°C) onto nitrocellulose membrane (BioRad, 0.45 μm), probed with primary and secondary antibodies according to the manufacturer's protocol, and immunodetected by using the ECL kit (Amersham Biosciences). The blots were scanned (UMAX Power Lock II, Dallas, TX) and quantified by an automated digitizing system UN-SCAN-IT GEL (Silk Scientific Corp, Orem, CT).

Endothelial cell migration

HPAECs (control and transfected by siRNA) cultured in 12- or 6-well plates to ~95% confluence were starved in 1% FBS EBM-2 medium for 3 h. The cell monolayer was wounded by scratching across the monolayer with a 10 μl standard sterile pipette tip. The scratched monolayer was rinsed twice with serum-free medium to remove cell debris and incubated for 16 h in 1% FBS EBM-2 under normoxia or hyperoxia. The area (~1 cm^2 total) in a scratched area was recorded at 0 and 16 h using a Hamamatsu digital camera connected to the Nikon Eclipse TE2000-S microscope with 10X objective and MetaVue software (Universal Imaging Corp., Sunnyvale, CA) and images were analyzed by the Image J software. The effect of hyperoxia on cell migration/wound healing was quantified by calculating the percentage of the free area not occupied by cells compared to an area of the initial wound that was defined as closure of wounded area.

Capillary tube formation (in vitro angiogenesis assay)

HPAECs, after silencing with Nox4 or Nox2 siRNA, were plated on growth factor-reduced Matrigel (basement membrane extract, Trevigen, Inc, Gaithersburg, MD), exposed to either normoxia or hyperoxia (95% O_2), and grown for 5 days. Endothelial growth medium was replaced every day and capillary tube formation and completion of ring like structures were recorded.

Transfection of siRNA for Nox4, Nox2, and $p22^{phox}$

To optimize conditions for efficient transfection, HPAECs were transfected with Fl-Luciferase GL2 Duplex siRNA (target sequence, 5′-CGTACGCGGAATACTTCGA-3′; Dharmacon) as a positive control. HPAECs, grown to ~60% confluence in 35-mm dishes, were transfected with Gene Silencer® (Gene Therapy System, Inc., San Diego, CA) transfecting agent plus with siRNA (50 n*M*) in serum-free EBM-2 medium according to the manufacturer's recommendation. After 3 h post-transfection, 1 ml of fresh complete EGM-2 medium containing 10% FBS was added, and cells were cultured for an additional 24–72 h for analysis of mRNA by real-time PCR and protein expression by Western blot analysis.

Transfection of Nox4 wild-type plasmid

For transient transfection, HPAECs grown in 6-well plates (~ 60% confluence), were transfected with Nox4 wt plasmid (1 μg of cDNA was mixed with 6 μl of Fugene 6/well in 1 ml of EGM), according to manufacturer's recommendations. After 3 h, the transfection medium was aspirated and 2 ml of complete EGM was added; cells were allowed to grow prior to exposure to either normoxia or hyperoxia for 48 h.

TABLE 1. RELATIVE mRNA EXPRESSIONS OF NADPH OXIDASE COMPONENTS AND PRIMER SEQUENCES

NADPH oxidase component	*Relative mRNA expression (normalized to 18S)*			
	HPAEC	*HLMVEC*	*Human gene*	*Primer sequence 5′ to 3′*
Nox1	0.079	0.061	Nox	+1: TTCACCAATTCCCAGGATTGAAGTGGATGGTC
Nox2	0.028	0.039		−2: GACCTGTCACGATGTCAGTGGCCTTGTCAA
Nox3	0.194	0.313	$gp91^{phox}$	+1: GTCACACCCTTCGCATCCATTCTCAAGTCAGT
Nox4	35.06	22.98		−2: CTGAGACTCATCCCAGCCAGTGAGGTAG
$p22^{phox}$	92.51	112.26	Nox3	+1: ATGAACACCTCTGGGGTCAGCTGA
$p40^{phox}$	0.003	0.086		−2: GGATCGGAGTCACTCCCTTCGCTG
$p47^{phox}$	0.1369	0.212	Nox4	+1: CTCGAGGAGCTGGCTCGCCAACGAAG
$p67^{phox}$	0.294	0.101		−2: GTGATCATGAGGAATAGCACCACCACCATGCAG
			$p22^{phox}$	+1: GGCGCTTCACCCAGTGGTACTTTGG
				−2: TAGGTAGATGCCGCTCGCAATGGC
			$p47^{phox}$	+1: AGTCCTGACGAGACGGAAGA
				−2: GGACGGAAAGTAGCCTGTGA
			$p67^{phox}$	+1: GGAGTGTGTCTGGAAGCAG
				−2: AGTGTGTAGGGCATGGAAC
			$p40^{phox}$	+1: GCTTCACCAGCCACTTTGTT
				−2: TCCTGTTTCACACCCACGTA

Animal procedures

Male Nox2$^{-/-}$(gp$^{91phox-/-}$) mice (background C57BL/6) and C57BL/6J mice were obtained from Jackson Laboratories, Bar Harbor, Maine. At 8 weeks of age, animals were exposed to either normoxia or hyperoxia for 24–72 h in a Plexiglass chamber designed for animal procedures. The chamber was supplied with 95% oxygen; oxygen saturation inside the chamber was monitored by an oxygen sensor (Pro ox 110, BioSpherix Inc, Redfield, NY). Mice were supplied with fresh water and Harlan Teklad diet. Animals which were weak and show symptoms of loss of weight were excluded from the study. Experiments conformed to the *Guide for the Care and Use of Laboratory Animals* published by the US National Institutes of Health (NIH publication No. 85-23) and were approved by the Institutional Animal Care and Use Committee of The University of Chicago. Bronchoalveolar lavage (BAL) was performed on mice with HBSS via a polyurethane catheter placed in the trachea. BAL fluid was collected on ice; cells from the lavage were analyzed by cytological techniques. At the end of the experiment, mice were anesthetized and lungs were perfused with fresh PBS several times; whole lungs without trachea were stored in liquid nitrogen. These samples were further processed for paraffin embedment, sectioning, and staining for Nox4 and Nox2 by the histological core facility at the University of Chicago. Tissue samples were processed for RNA using a polytron homogenizer (Brinkmann Gmbh, Westbury, NY) with Trizol (Invitrogen). For assessment of lung capillary leakage, Evans blue dye (EB) (20 mg/kg) was injected into the internal jugular vein 30 min before the termination of the experiment to assess vascular leak. The lungs were perfused free of blood (perfusion pressure, 5 mm Hg) with phosphate-buffered saline (PBS) containing 5 m*M* ethylenediaminetetraacetic acid, via thoracotomy, excised *en bloc*, blotted dry, weighed, and snap-frozen in liquid nitrogen. The right lung was homogenized in PBS (1 ml/100 μg tissue), incubated with

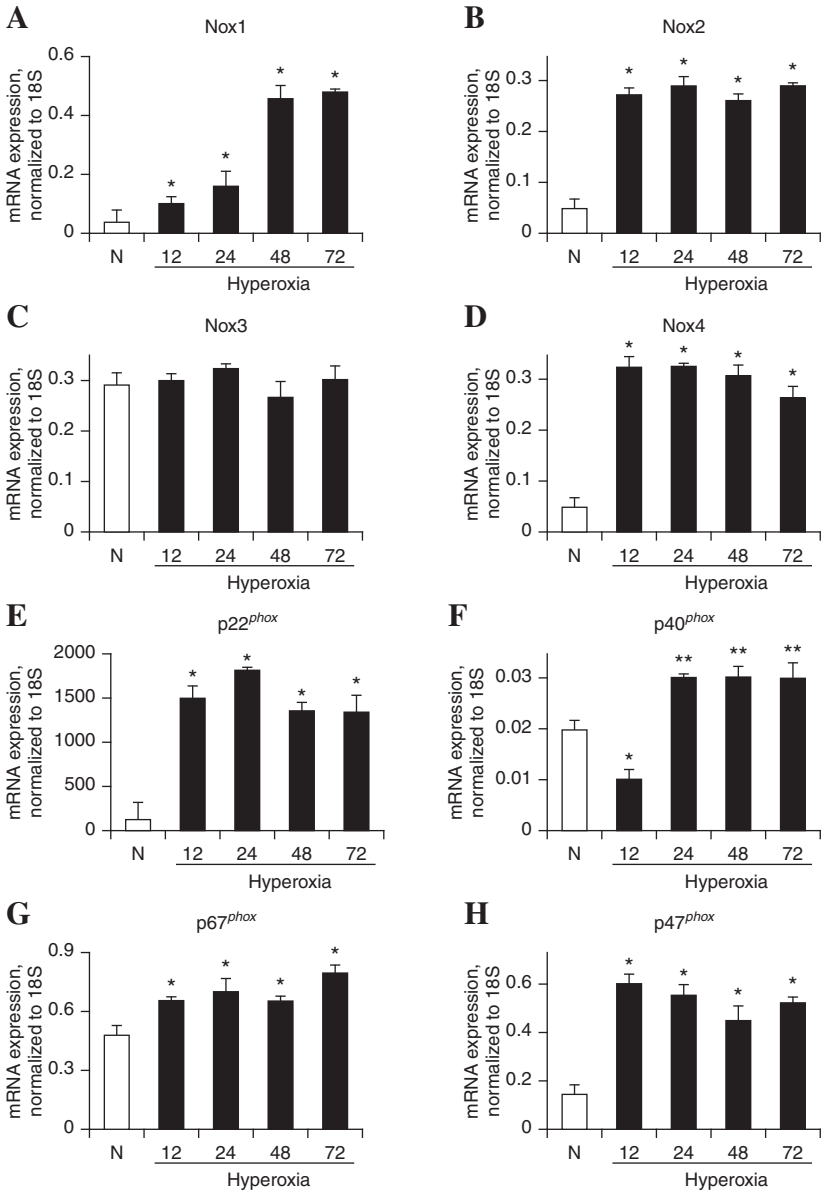

FIG. 1. Effect of hyperoxia on mRNA expression of Nox and phox family NADPH oxidases in HPAECs. HPAECs grown to ~90% confluence were exposed to normoxia (room air) or hyperoxia (95% O_2) for 12, 24, 48, and 72 h. Total RNA was extracted and expressions of Nox and phox homologues were quantified by real-time RT-PCR and normalized with 18S rRNA. The values are mean ± S.E.M for three independent experiments. *significantly different from normoxia ($p < 0.05$); **significantly different from normoxia ($p < 0.01$).

2 volumes of formamide (18 h, 60°C), and centrifuged at 5,000 *g* for 30 min. The optical density of the supernatant was determined spectrophotometrically at 620 nm. The extravasated EB concentration in lung homogenate was calculated against a standard curve (micrograms Evans blue dye per lung).

Statistical analyses

Analysis of variance and Student–Newman–Keul's test were used to compare means of two or more different treatment groups. The level of significance was set to $p < 0.05$ unless otherwise stated. Results are expressed as mean ± S.E.M.

Results

Expression of Nox and phox family NADPH oxidase components in HPAECs under normoxia and hyperoxia

At least twelve components of nonphagocytic and phagocytic NADPH oxidases have been identified in Genebank. To study the expression of these homologues in human vascular endothelium by real-time RT-PCR, specific primers were designed (Table 1). Analyses of the total RNA by real time RT-PCR, normalized to 18S rRNA, show that HPAECs and HLMVECs express most of the NADPH oxidase components, namely, Nox2 (gp91^{phox}), p47^{phox}, p67^{phox}, p40^{phox}, and p22^{phox}, and the recently described Nox1, Nox3, and Nox4 homologues (Table 1). However, expression of Nox5 was not detected by real-time RT-PCR, under similar gene amplification cycles. Among the Nox family NADPH oxidases, expression of Nox4 was significantly higher (~1,000 fold) compared to Nox1, Nox2, and Nox3. In both HPAECS and HLMVECs, the expression of p22^{phox} was 3- to 5-fold higher compared to Nox4, whereas the expression of p40^{phox}, p47^{phox} , and p67^{phox} were lower (Table 1).

Since hyperoxia stimulates activation of NADPH oxidase and ROS/$O_2^{\cdot -}$ production in vascular endothelium (4), and causes lung injury (26), we investigated the effect of exposure of hyperoxia (95% oxygen) on the mRNA expression of *Nox* and *phox* components of NADPH oxidase. As shown in Fig. 1, exposure of HPAECs to hyperoxia for 12–72 h increased the mRNA expressions of Nox4 and p22^{phox}, as determined by real-time RT-PCR normalized to 18S rRNA. However, changes in the expression of Nox1, Nox2, p40^{phox}, and p47^{phox}, in response to hyperoxia, were much lower compared to Nox4 and p22^{phox} (Fig. 1). The mRNA profiles of Nox4, Nox2, and p22^{phox}, under normoxia and hyperoxia, were validated by Western blot analysis, which showed increased protein expressions of Nox4 (~65kDa) at 3 and 24 h of hyperoxia (Fig. 2A), while Nox2 protein expression was enhanced only at 24 h of exposure to hyperoxia (Fig. 2B). Further, hyperoxia (3 or 24 h) enhanced the mRNA levels of p22^{phox} several fold as compared to normoxic cells; however, change in the protein expression of p22^{phox} by hyperoxia (3 or 24 h) was ~1.4-fold (Fig. 2C).

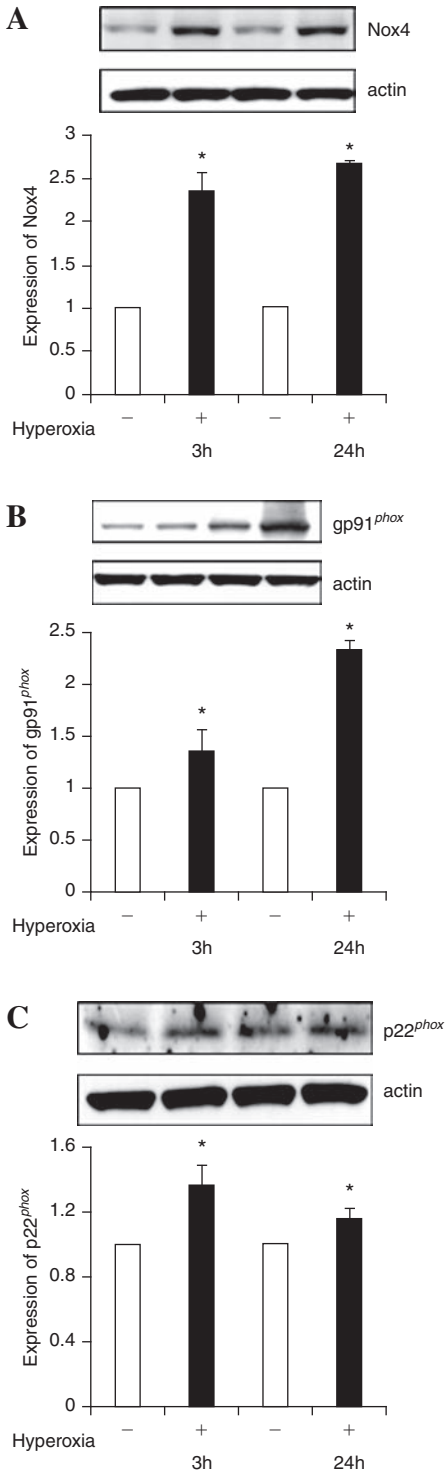

FIG. 2. Hyperoxia increases protein expression of Nox4 and Nox2 in HPAECs. HPAECs (~90% confluence) were subjected to normoxia or hyperoxia for 3 or 24 h. Cells were rinsed twice in ice-cold PBS , total cell lysates (20 μg of protein) were subjected to SDS-PAGE, as described in "Materials and Methods" and analyzed by Western blot analysis with anti-Nox4 (Santa Cruz, CA), -Nox2 (gp91^{phox}), and -p22^{phox} antibodies. Shown are representative Western blots from three independent experiments. Blots were scanned and quantified by automated digitized system UN-SCAN-IT-GEL. *significantly different from cells exposed to normoxia ($p < 0.05$).

Effect of hyperoxia on localization of Nox4 and p22^{phox} in HPAECs

There are reports on the localization of Nox4 either in endoplasmic reticulum or nucleus of mammalian cells (20, 41). Therefore, immunofluorescence studies were carried out to determine the localization of Nox4 and p22^{phox} in HPAECs under conditions of normoxia and hyperoxia. As shown in Fig. 3A, Nox4 was primarily localized in cell nucleus under normoxia, and exposure of cells to hyperoxia (3 or 24 h) resulted in redistribution of Nox4 to the cytoplasm and plasma membrane as determined by confocal microscopy. In contrast to Nox4, p22^{phox} was localized to structures resembling endoplasmic reticulum in normoxia and in punctate nuclear structures after exposure to hyperoxia (Fig. 3A). Additionally, merging of the immunofluorescence stains of Nox4 (green) and p22^{phox} (red) showed colocalization (yellow) in the nucleus under hyperoxia (Fig. 3A). The nuclear immunolocalization of Nox4 and p22^{phox} was confirmed by isolation of enriched nuclear fraction and Western blot analysis for Nox4 and p22^{phox}. As shown in Fig. 3B, Western blot analysis of the cytoplasm and isolated nuclear fractions revealed higher levels of Nox4 in the nucleus compared to the cytoplasm fraction. Further, nuclear fraction also showed staining for p22^{phox} by Western blotting. The purity of the isolated nuclear preparation was verified by expression of lamin B1 (nuclear cytoskeletal protein), absence of lactate dehydrogenase (cytoplasmic enzyme), and calreticulin (marker of endoplasmic reticulum). Further, exposure of HPAECs to hyperoxia for 3 or 24 h increased the protein expression of Nox4 in the nuclear and cytoplasmic fractions (Fig. 3B); however, no such increase in the expression of p22^{phox} in the nuclear fraction was observed after 3 h hyperoxia. Interestingly, the expression of p22^{phox} was also enhanced at 24 h of hyperoxia (Fig. 3B). Under similar exposure to hyperoxia (3 or 24 h), nuclear localization of Nox2 and p47^{phox} was not detected (data not shown). To further confirm the nuclear localization of Nox4, expression of Nox4 was downregulated by transfection of HPAECs with Nox4 siRNA (50 n*M*) for 48 h, which reduced the mRNA and protein expression of Nox4 (>90%) as determined by real-time RT-PCR and Western blot analysis (Fig. 4A). Analyses of Nox4 siRNA transfected HPAECs by immunofluorescence microscopy and Western blot analysis of nuclear fraction also revealed a decrease in Nox4 expression compared to cells transfected with scrambled siRNA (Fig. 4B and C). These results show a nuclear colocalization of Nox4 and p22^{phox} during hyperoxia in HPAECs.

Role of Nox4 in hyperoxia-induced ROS generation

Our earlier results show that hyperoxia-induced ROS/$O_2^{\cdot -}$ production was dependent upon activation of NADPH oxidase, rather than mitochondrial electron transport (27), and Nox2 siRNA partly blocked hyperoxia-induced ROS generation in HPAECs (37). To study the functional role of Nox4 in hyperoxia-induced ROS/$O_2^{\cdot -}$, Nox4 expression was downregulated with Nox4 siRNA or upreg-

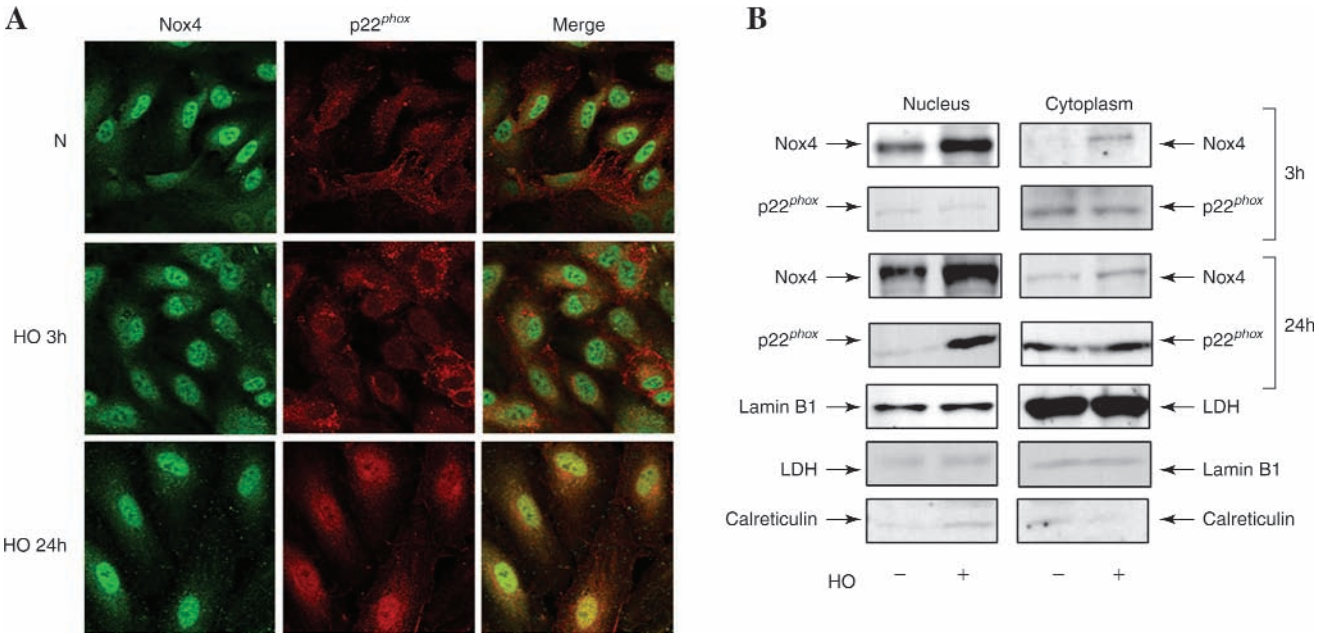

FIG. 3. Localization of Nox4 and p22^{phox} under normoxia and hyperoxia in HPAECs. (**A**) HPAECs grown on glass coverslips were exposed to normoxia (N) or hyperoxia (HO) for 3 h, washed, fixed, permeabilized and probed with anti-Nox4 (from Dr. Lambeth) or anti-p22^{phox} antibodies. Hyperoxia induced association of Nox4 with p22^{phox} protein (*yellow in merged image*) shown is a representative confocal immunofluorescence image from three independent experiments. (**B**) HPAECs in 100-mm dishes grown to ~90% confluence were exposed to normoxia or hyperoxia for 3 or 24 h. Nuclear and cytoplasmic fractions were prepared using Active Motif according to manufacturer's protocol as described in "Materials and Methods." Lysates from nuclear and cytoplasmic fractions (20 μg protein) were subjected to SDS-PAGE and Western blot analysis with antibodies against Nox4 (Santa Cruz, CA), p22^{phox}, Lamin B1, lactate dehydrogenase (LDH), and calreticulin. Representative blots from three independent experiments are shown. (For interpretation of the references to color in this figure legend, the reader is referred to the web version of this article at www.liebertonline.com/ars).

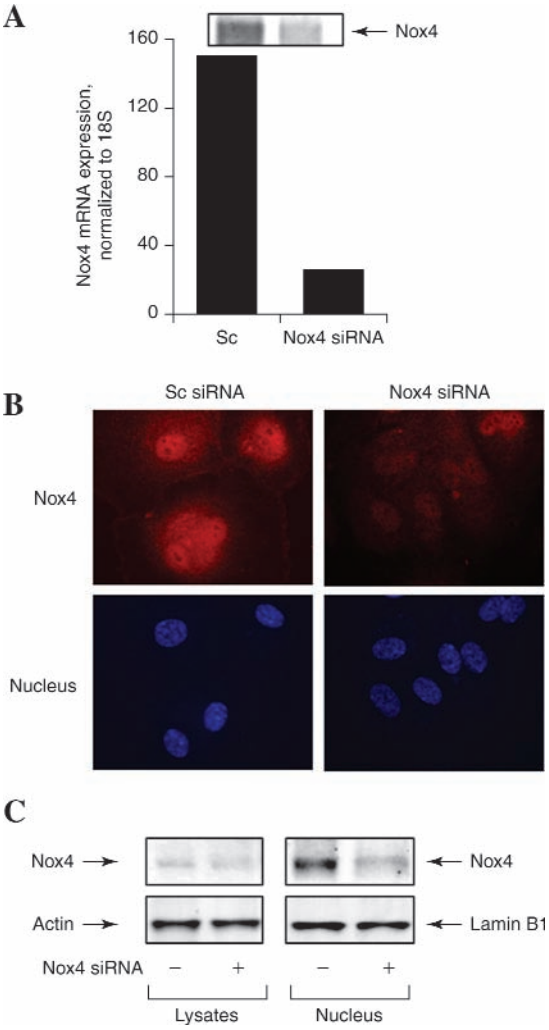

FIG. 4. Nox4 siRNA attenuates hyperoxia induced expression of Nox4 in nucleus. HPAECs grown on 35-mm dishes (**A** and **C**) or glass coverslips (**B**) to ~50% confluence were transfected with scrambled siRNA (Sc) or Nox4 siRNA (50 n*M*) for 48 h. (**A**) Total RNA was extracted and Nox4 mRNA expression was quantified and normalized to 18S rRNA by real-time RT-PCR. Values are average of three independent determinations. (**B**) Sc or Nox4 siRNA transfected cells were exposed to normoxia or hyperoxia (3 h), washed, fixed, permeabilized, and probed with anti-Nox4 antibody (from Dr. Lambeth) or DAPI for nuclear staining and examined by immunofluorescence microscopy using a 60X oil objective. The Nox4 (*red*) and DAPI (*blue*) images show matched cell fields for each condition. A representative image from several independent experiments is shown. (**C**) Isolated nuclear or cytoplasmic fraction (20 μg protein) were subjected to SDS-PAGE and probed with anti-Nox4 (Santa Cruz, CA), or anti-β actin or -lamin B1 antibodies. Representative blots from three independent experiments are shown. (For interpretation of the references to color in this figure legend, the reader is referred to the web version of this article at www.liebertonline.com/ars).

ulated with Nox4 wild-type plasmid. Nox4 downregulation decreased hyperoxia-induced oxidation of DCFDA fluorescence (ROS production), and hydroethidine fluorescence ($O_2^{\cdot -}$ generation) by ~30% compared to scrambled siRNA transfected cells exposed to hyperoxia (Fig. 5A and B). Interestingly, Nox4 siRNA slightly blocked DCFDA oxidation/hydroethidine fluorescence under normoxia (Fig. 5A and B). Furthermore, the siRNA for Nox4 was specific as it did not affect expression of Nox1/Nox3 in HPAECs (results not shown). Overexpression of Nox4 wild-type plasmid increased oxidation of DCFDA fluorescence (ROS production) by ~1.8 fold compared to vector control cells under normoxia and Nox4 wild-type overexpression further enhanced hyperoxia-induced DCFDA oxidation (Fig. 5C). Further, pretreatment of cells with PEG-SOD almost completely blocked hyperoxia-induced ROS/$O_2^{\cdot -}$ production (Fig. 5A and B) Taken together, these results suggest a role for Nox4 in hyperoxia-induced ROS/$O_2^{\cdot -}$ generation in HPAECs.

Hyperoxia-induced ROS production by nuclear Nox4

As Nox4 is predominantly localized in nucleus of HPAECs, next we investigated the role of nuclear Nox4 in ROS/$O_2^{\cdot -}$ production by monitoring generation of H_2O_2 production/hydroethidine fluorescence under basal and hyperoxic conditions. Nuclei isolated from scrambled or Nox4 siRNA transfected cells were exposed to normoxia or hyperoxia (3 h). As shown in Fig. 6A, exposure of nuclei from scrambled siRNA transfected cells to hyperoxia (3 h) accumulated H_2O_2 (~2-fold) compared to normoxic nuclei while Nox4 siRNA transfected nuclei exhibited reduced H_2O_2 production. Interestingly, downregulation of Nox4 expression by siRNA reduced basal ROS production under normoxia (Fig. 6A). Further, cells incubated with hydroethidine showed a pronounced increase in nuclear hydroethidine fluorescence, compared to normoxic cells, at 3 h after hyperoxia exposure, and downregulation of Nox4 with Nox4 siRNA, but not scrambled siRNA, reduced basal and hyperoxia-induced hydroethidine oxidation in the nucleus (Fig. 6B). Quantitation of the images showed ~2.5-fold increase over baseline in nuclear hydroethidine fluorescence in hyperoxia and downregulation of Nox4 reduced hyperoxia-induced nuclear hydroethidine fluorescence to ~1.5-fold change (Fig. 6C). Similarly, Nox4 siRNA reduced cytoplasmic hydroethidine fluorescence (~1.3-fold) *versus* Nox4 siRNA transfected cells (~0.2-fold) at 3 h after hyperoxia (data not shown). These results suggest a potential role for nuclear Nox4 in generating ROS/$O_2^{\cdot -}$ due to hyperoxia in HPAECs.

Knockdown of Nox2 and Nox4 by siRNA upregulates expression of Nox4 and Nox2, respectively, in HPAECs

Although Nox4 siRNA did not alter the expression of Nox1 and Nox3 levels, expression of Nox2 mRNA was upregulated on silencing Nox4 while Nox4 mRNA and protein expression were enhanced after knockdown of Nox2 (Fig. 7A and B). Numerous attempts of simultaneous transfection of Nox2 and Nox4 in HPAECs resulted in increased cell death within 48 h (results not shown). Interestingly, siRNA-mediated knockdown of $p22^{phox}$ increased Nox4 mRNA levels by ~2-fold (Fig. 7C). A similar compensatory mechanism between Nox4 and Nox2 after siRNA treatment was observed in human cardiac ECs; however, in primary human bronchial epithelial cells and in adenocarcinoma cell line A549, knockdown of Nox2 and Nox4 by siRNA did not upregulate the expression of Nox4 or Nox2, respectively (data not shown). These results show for the first time the ability of lung ECs to reciprocally compensate for Nox2 or Nox4 deficiency.

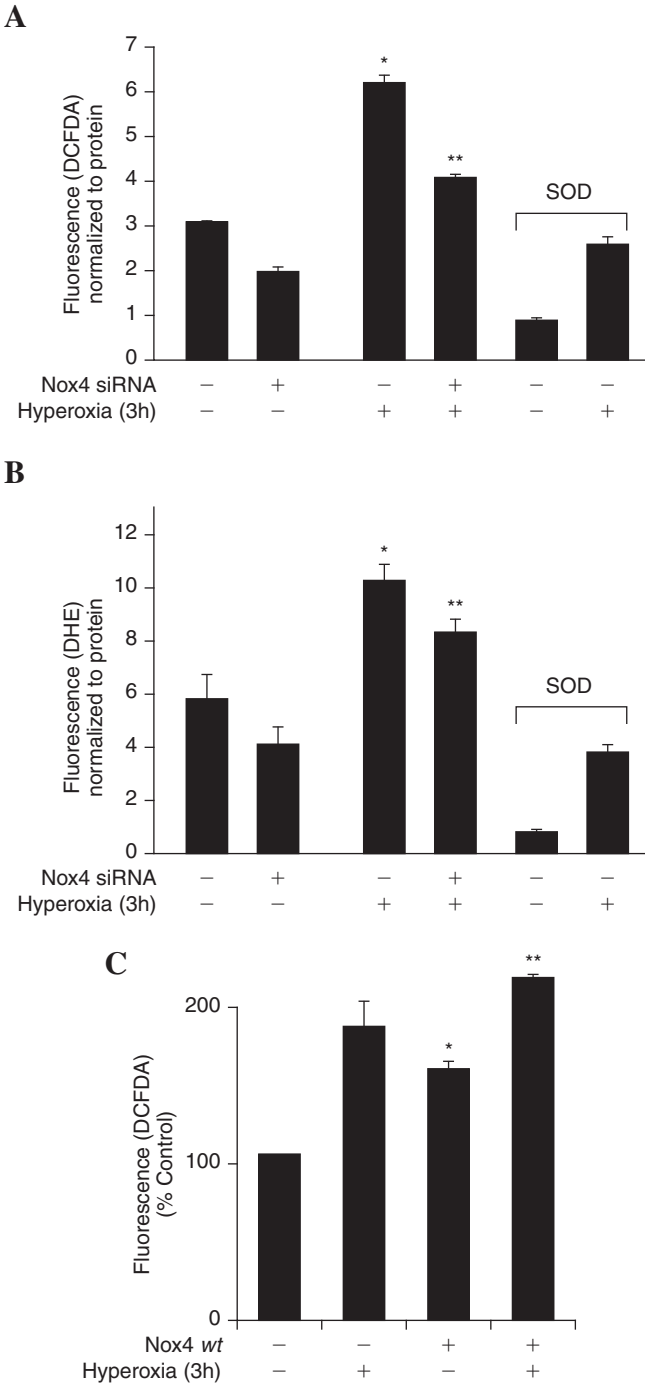

FIG. 5. Role of Nox4 in hyperoxia-induced ROS generation. (**A** and **B**) HPAECs grown to ~50% confluence in 35-mm dishes were transfected with scrambled siRNA or Nox4 siRNA (50 n*M*) for 48 h as described in "Materials and Methods." After 48 h, cells were pretreated with medium alone or medium containing PEG-conjugated SOD at 400 Units/mL for 1 h prior to addition of 10 μM DCFDA (**A**) or hydroethidine (**B**) for 30 min and washed once in basal medium. Cells in **A** or **B** were exposed to normoxia or hyperoxia (3 h) and at the end of the exposure, formation of total ROS (**A**) or superoxide (**B**) was measured by spectrofluorimetry. Values are mean ± S.E.M from three independent experiments done in triplicate and normalized to total protein. *significantly different from normoxia ($p < 0.05$); **significantly different from scrambled siRNA transfected cells exposed to hyperoxia ($p < 0.01$). (**C**) HPAECs grown to ~70% confluence on 35-mm dishes were transfected with 1 μg of plasmid DNA/ml of Nox4 wild type. 72 h later, cells were loaded with 10 μM DCFDA for 30 min, washed once in basal medium and exposed to normoxia or hyperoxia (3 h). Total ROS production was visualized under immunofluorescence microscopy and quantified as described in "Materials and Methods." Values are mean ± S.E.M of three independent experiments. *significantly different from normoxia ($p < 0.05$); **significantly different from vector control transfected cells under normoxia ($p < 0.01$).

Effect of hyperoxia on lung injury and expression of Nox4 in control and Nox2 (gp91^{phox}) $^{-/-}$ mice

Male C57BL/6J or Nox2$^{-/-}$ mice with similar genetic background were exposed to normoxic air or 95% oxygen (hyperoxia) for 72 h, and at various times, mice from both groups were evaluated for alveolar-capillary membrane dysfunction by determining protein levels in bronchoalveolar lavage (BAL) and Evans Blue (EB) dye extravasation. As shown in Fig. 8A, BAL fluid from mice exposed to hyperoxia for 48 and 72 h had significantly higher protein levels compared to normoxic animals. BAL from hyperoxia-exposed control mice exhibited higher cell counts with increased percentage of macrophages (Fig. 8C). Further, histopathology of lung sections revealed pulmonary injury induced by hyperoxia, as evidenced by increased numbers of fibroblasts and fibrosis (Fig. 8D). Since hyperoxia causes vascular leak in C57BL/6J mice, next we investigated a role for NADPH oxidase in hyperoxic lung injury using genetically altered Nox2$^{-/-}$ null mice. Under normoxic conditions, mice in both the groups showed similar BAL protein levels, however, in hyperoxia the control mice exhibited increased alveolar and vascular leakiness (Fig. 8A and B), and influx of neutrophils into alveolar space compared to the mice with

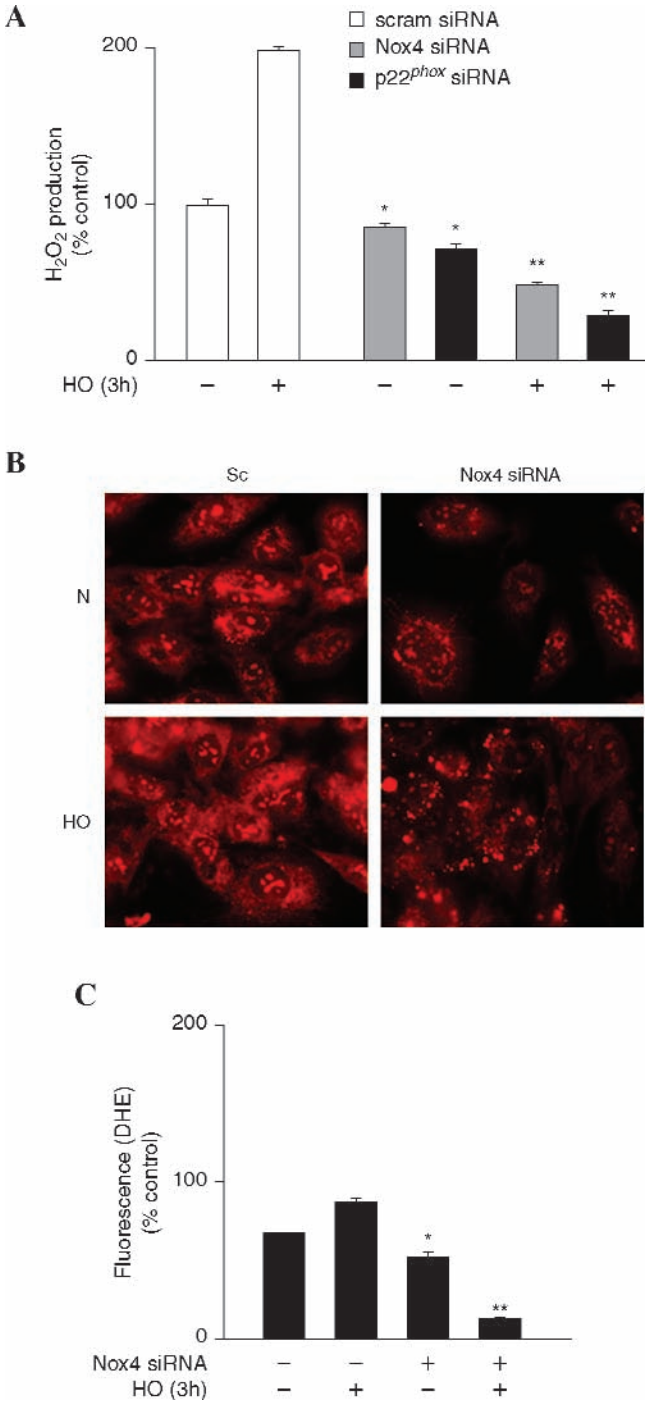

FIG. 6. Role of]Nuclear Nox4 in hyperoxia-induced ROS generation. (**A**) HPAECs grown to ~50% confluence in 100-mm dishes were transfected with scrambled siRNA or Nox4 siRNA (50nM) or $p22^{phox}$ siRNA (50 n*M*) for 48 h. Nuclear fractions were prepared as described in "Materials and Methods" and exposed to normoxia or hyperoxia for 3 h. Accumulation of H_2O_2 was measured using an Amplex Red assay. Values are mean ± S.E.M from three independent experiments and expressed in % control. *significantly different from scrambled siRNA normoxic nuclear fraction ($p < 0.05$), **, significantly different from scrambled siRNA normoxic nuclear fraction ($p < 0.01$). (**B** and **C**) HPAECs grown to ~50% confluence in glass-bottom dishes were transfected with scrambled siRNA or Nox4 siRNA (50 n*M*) for 48 h. Cells were loaded with10 μM hydroethidine for 30 min and washed once with basal medium, and further exposed to normoxia or hyperoxia for 3 h. Formation of superoxide and enhanced intercalation of oxidized hydroethidine with nuclear DNA was visualized under fluorescence microscopy and quantified. Values are mean ± S.E.M from three independent experiments in triplicates and expressed as % control. *significantly different from scrambled siRNA transfected cells under normoxia ($p < 0.05$), **significantly different from scrambled siRNA transfected cells under normoxia ($p < 0.01$). (For interpretation of the references to color in this figure legend, the reader is referred to the web version of this article at www.liebertonline.com/ars).

targeted disruption of Nox2 (Fig. 8C), suggesting a role for Nox2 in hyperoxia-mediated vascular leakiness. Interestingly, exposure of $Nox2^{-/-}$ mice to hyperoxia still caused significant vascular leak as measured by increased BAL fluid protein, infiltration of macrophages in BAL fluid, and Evans Blue dye extravasation (Fig. 8A, B, and C), suggesting potential involvement of other Nox family homologues, such as Nox4, in mediating lung injury.

Having demonstrated that silencing Nox4 and Nox2 upregulates the expression of Nox2 and Nox4, respectively, we next investigated the expression of Nox4 in $Nox2^{-/-}$ mice and the effect of hyperoxia on Nox4 expression in the lungs of control and $Nox2^{-/-}$ mice. Analyses of total lung tissue mRNA by real-time RT-PCR confirmed low expression of Nox2, compared to Nox4 in control mice (Fig. 9A), and exposure of control mice to hyperoxia for 48 h increased the expression of Nox2 (relative mRNA expression, normalized to 18S rRNA, from 0.02 to 0.04), and Nox4 (relative mRNA expression, normalized to 18S rRNA, from 75 to 300) (Fig. 9A). In $Nox2^{-/-}$ mice, as expected, there was no expression of Nox2 mRNA; however, the expression of Nox4 mRNA was higher compared to control mice

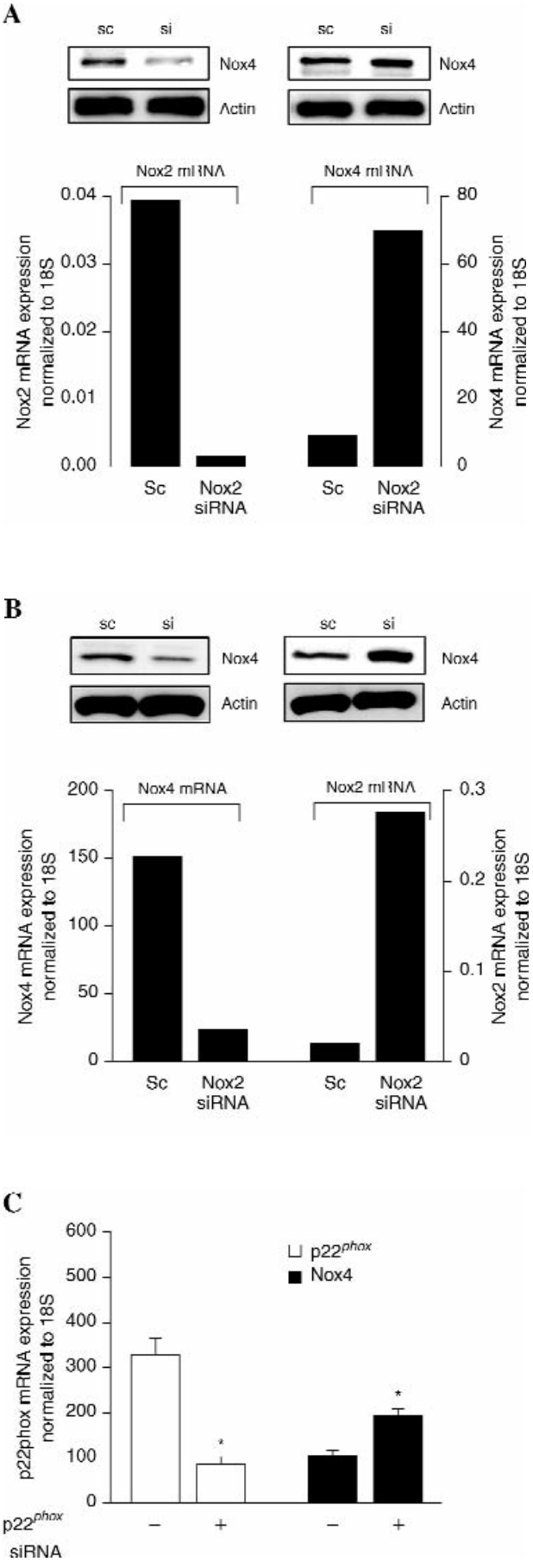

under normoxia (control mice, Nox4 expression 75 *vs.* Nox2$^{-/-}$ mice, Nox4 expression, 225 all normalized to 18S rRNA) (Fig. 9B). Further exposure of Nox2$^{-/-}$ mice to hyperoxia did not upregulate the expression of Nox4, in contrast to the control mice (Fig. 9B). These results from *in vivo* experiments show upregulation of Nox4 expression in Nox2$^{-/-}$ mice and exposure of Nox2$^{-/-}$ mice to hyperoxia did not further enhance the expression of Nox4, as compared to control mice. Histological evaluation of sections of lung from both wild-type mice and Nox2$^{-/-}$ (Fig. 9C) show the increased Nox2 and Nox4 expression with hyperoxia (24 h) (brown staining, DAB, see Materials and Methods). However, expression of Nox4 in Nox2$^{-/-}$ mice was higher compared to wild-type mice under normoxia, and exposure to hyperoxia did not further increase Nox4 expression (Fig. 9C).

Nox2 and Nox4 mediate hyperoxia-induced migration and capillary tube formation in HPAECs

Having established a role for Nox4 in hyperoxia-induced ROS/$O_2^{\cdot -}$ generation in HPAECs, we next determined the functional significance of the ROS production in cell migration and capillary tube formation. Exposure of HPAECs to hyperoxia (16 h) increased migration (Fig. 10A), which was blocked by *N*-acetylcysteine (NAC) (Fig. 10A, lower panel). Further, NAC attenuated hyperoxia-induced ROS generation in HPAECs (Fig. 10B). Next, we investigated the role of Nox4 and Nox2 in EC motility and capillary tube formation. In these experiments, 35-mm dishes were seeded with the same number of cells ($\sim 5 \times 10^4$) and at 50–60% confluence, cells were transfected with scrambled siRNA or Nox4 or Nox2 siRNA. At the end of 48 h, both the scrambled and siRNA transfected cells reached similar confluence, indicating that downregulation of Nox4 or Nox2 did not affect cell growth/proliferation in HPAECs (data not shown). However, transfection of HPAECs with Nox4 or Nox2 siRNA attenuated hyperoxia-induced migration and capillary tube formation, compared to control cells transfected with scrambled siRNA (Figs. 11 and 12). These results support a role for Nox4- and Nox2-dependent generation of ROS in hyperoxia-induced migration and capillary tube formation in lung ECs.

FIG. 7. Silencing of Nox2 and Nox4 by siRNA upregulates expression of Nox4 and Nox2, respectively. HPAECs grown on 35-mm dishes to ~50% confluence were transfected with 50 n*M* scrambled siRNA or Nox2 siRNA or Nox4 siRNA or p22^{phox} siRNA for 48 h. (**A** and **B**) Total RNA was isolated and mRNA levels of Nox2 and Nox4 were quantified by real-time RT-PCR and normalized to 18S rRNA. In parallel experiments, total cell lysates (20 μg protein) from scrambled siRNA or Nox2 siRNA or Nox4 siRNA transfected cells were subjected to SDS-PAGE and Western blotted anti-Nox4 (Santa Cruz, CA) (**A**) or anti-Nox2 (**B**) antibodies. Values are average of three independent experiments. Shown are representative of blots from three separate experiments. (**C**) Total RNA was isolated and mRNA levels of p22^{phox} were determined by real-time RT-PCR and values are average of three independent experiments.

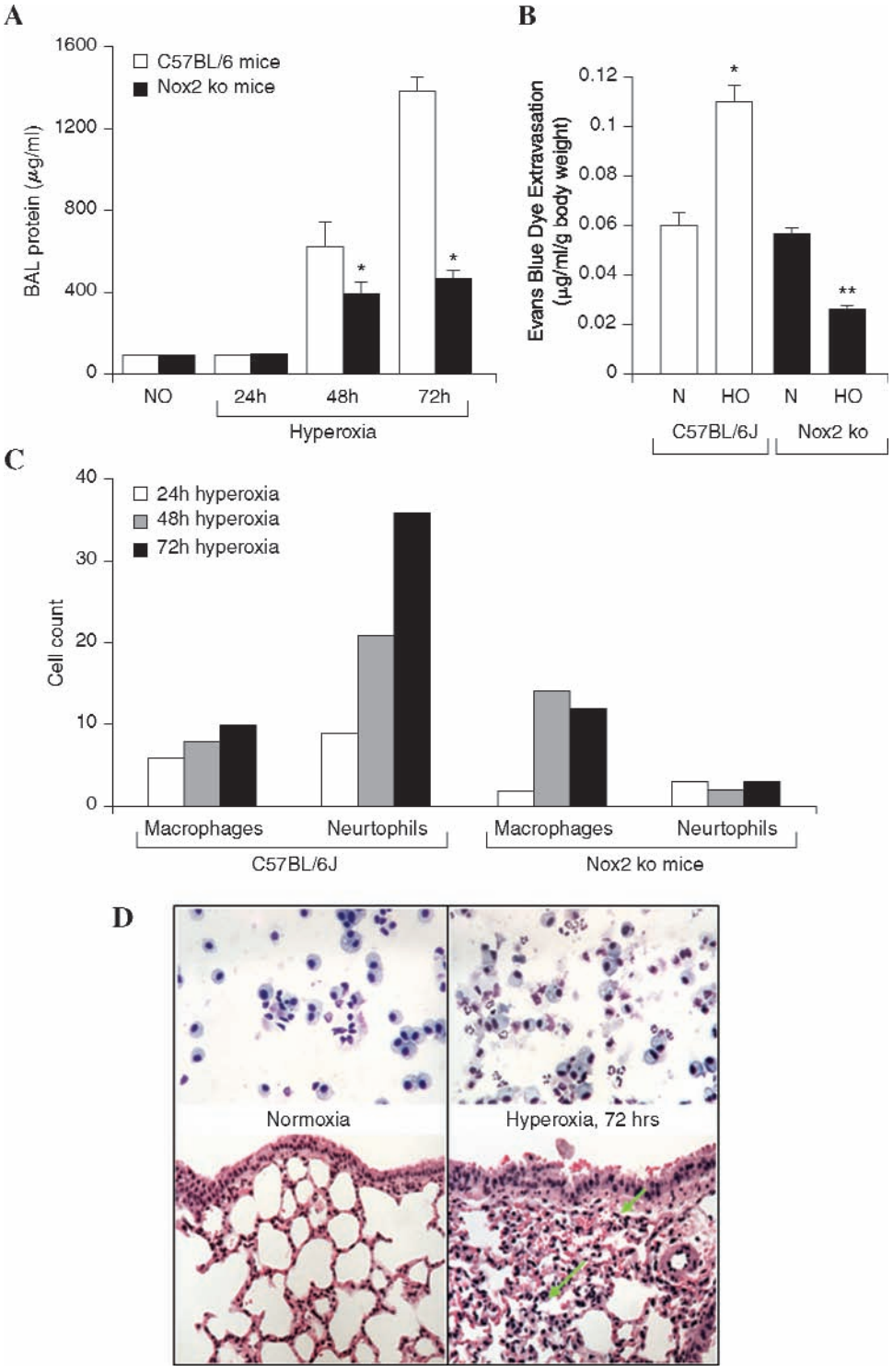

FIG. 8. Effect of hyperoxia on lung injury in C57BL/6J and Nox2$^{-/-}$ mice. (**A**) C57BL/6J mice or Nox2$^{-/-}$ mice were exposed to normoxia (room air-21% oxygen) or hyperoxia (95% oxygen) for 24, 48, and 72 h. Mice were anesthetized by intraperitoneal injection of 30 μl of ketamine (100 mg/kg)/xylazine (10 mg/kg). BAL (bronchoalveolar lavage) fluid was aspirated from the lungs and stored on ice before measuring total protein. Each group had five mice and values are mean ± S.E.M of three independent experiments. (**B**) The levels of extravasated Evans blue dye (μg/ml/g body weight) in mouse lung homogenate of wild type and Nox2$^{-/-}$ mice are shown. Values are mean ± S.E.M of three independent experiments. (**C**) BAL fluids were centrifuged at 200 *g* for 10 min, and the pellet was immediately resuspended in physiological saline for total cell counts. Differential cell counts were carried out in the centrifuged cells after Wright–Giemsa staining. (**D**) shows the histological staining of the lung tissue from mice exposed to normoxia or hyperoxia. Lung tissues were stored in formalin for 24 h before processing to cut and mount the section for staining with H&E. Shown is a representative staining of the lung tissue from three independent determinations. (For interpretation of the references to color in this figure legend, the reader is referred to the web version of this article at www.liebertonline.com/ars).

Discussion

The present study supports a role for Nox4 in hyperoxia-induced ROS/$O_2^{\cdot -}$ generation in HPAECs. Our results indicate that ROS generated via Nox4 and Nox2 regulates hyperoxia-induced EC migration and capillary tube formation. Our results also show that independent downregulation of Nox4, and Nox2 with siRNA upregulated the mRNA and protein expression of Nox2 and Nox4, respectively, in HPAECs. This novel compensatory mechanism between Nox4 and Nox2 expression was also evident in Nox2$^{-/-}$ mice that exhibit increased levels of basal Nox4 expression compared to control wild-type mice.

ROS generated by the Nox family of NADPH oxidases have emerged as an important regulatory and signaling molecule modulating vascular cell growth, migration, cytoskeletal organization, and barrier function (31). Among the five Nox homologues, namely Nox1, Nox2, Nox3, Nox4, and

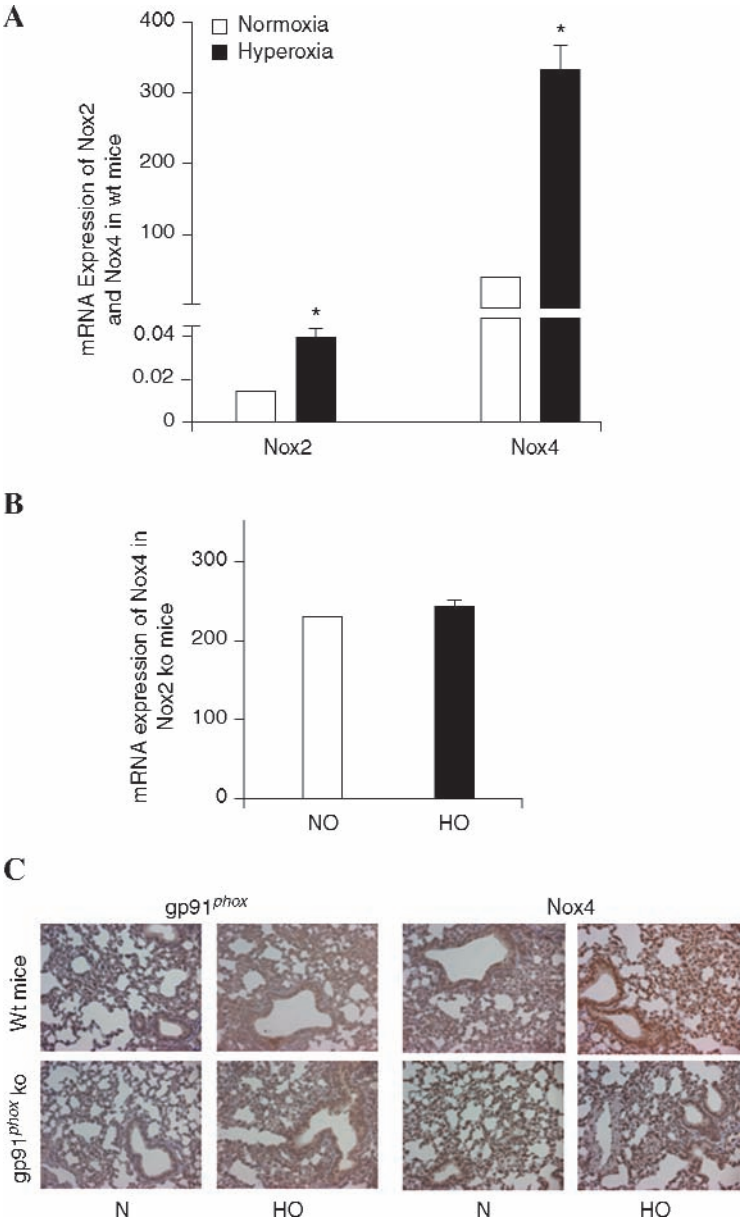

FIG. 9. Effect of hyperoxia on Nox4 mRNA expression and immunohistochemical staining of control and Nox2$^{-/-}$ mice. (**A**) Lung tissues were harvested from wild-type-C57BL/6J mice exposed to normoxia or hyperoxia (24 h). Total RNA was isolated, Nox2 and Nox4 mRNA were quantified by real-time RT-PCR and normalized to 18S rRNA. *significantly different from normoxic lung tissue ($p < 0.05$). (**B**) Nox2$^{-/-}$ mice were exposed to either normoxia or hyperoxia (95% O_2 for 24 h). Total RNA was isolated and mRNA levels of Nox4 were quantified by real-time RT-PCR and normalized to 18S rRNA. (**C**) Lung tissues from wild-type and Nox2$^{-/-}$ mice were stained with Nox2 and Nox4 antibodies using standard immunohistochemistry (immuno-peroxidase) techniques. (For interpretation of the references to color in this figure legend, the reader is referred to the web version of this article at www.liebertonline.com/ars).

Nox5 that have been identified in mammalian cells and tissues (19), Nox2 is predominantly present in neutrophils. Nox4, first identified in the kidney, is highly expressed in vascular ECs and smooth muscle cells (32). Our results show that Nox4 is the most abundant isoform expressed in HPAECs and HLMVECs, confirming the earlier reports of higher Nox4 expression in HUVECs and vascular smooth muscle cells (10). Although Nox4 mRNA expression in HPAECs and HLMVECs was ~1,000 fold higher compared to Nox2 expression, and Western blot analyses revealed that both Nox4 and Nox2 exhibit similar levels of protein expression. Protein expression is dictated by several factors, including level of mRNA half life, translation, and turnover rate of the protein of interest. It is evident that there is no direct correlation between mRNA expression levels and protein expression, and in many instances, an increase in mRNA expression does not necessarily translate to similar level of protein expression (12, 14). In HPAECs, hyperoxia (24 h) increased mRNA levels by ~8-fold compared to normoxia; however, the protein expression was enhanced by ~3-fold after hyperoxia.

In the vasculature, Nox-derived ROS have been implicated in a variety of cellular responses under normal and pathological conditions. Nox1-derived $O_2^{\cdot -}$ production by advanced glycation endproducts activate NF-kB-dependent iNOS in rat thoracic aorta smooth muscle cells (30), and a recent study suggests a strong link between Nox1-derived ROS by angiotensin II and a hypertensive signaling element in vasculature (21). Whereas Nox2-derived ROS by activated leukocytes have been functionally linked to host defense against bacterial infections (1), the function of Nox4- and Nox2-derived ROS in the vasculature appears to be complex and dependent on the relative expression levels of the Nox isoforms, and the type(s) of vascular cells involved. Nox2-

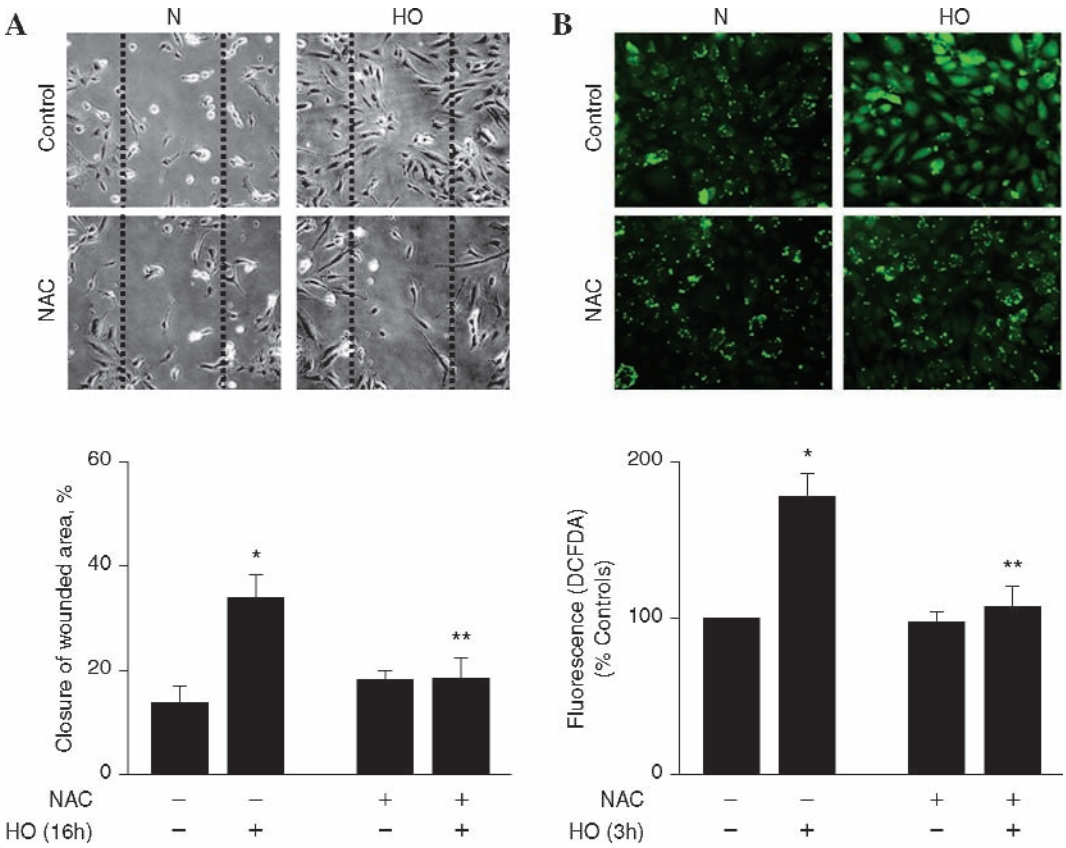

FIG. 10. ***N*-acetylcysteine attenuates hyperoxia-induced ROS generation and wound healing.** HPAECs grown on 35-mm dishes (**A**) or glass coverslips to ~90% confluence were pretreated with vehicle or vehicle plus *N*-acetylcysteine (NAC) 1 m*M* for 60 min. (**A**) Cells were wounded by scratching across the monolayer with a 10 μl sterile pipette tip. The scratched monolayers were rinsed twice in serum-free medium and exposed to either normoxia (N) or hyperoxia (HO) for 16 h. The effect of NAC on hyperoxia-mediated cell migration was quantified by calculating the % of free area not occupied by cells adjacent to an area of the initial wound that was defined as closure of wounded area as described in "Materials and Methods." Values are mean ± S.E.M of three independent experiments in triplicates. *significantly different from normoxia and without NAC ($p < 0.05$); **significantly different from cells exposed to hyperoxia without NAC ($p < 0.01$). (**B**) After NAC pretreatment for 1 h, cells were loaded with 10 μM DCFDA for 30 min, washed once in basal medium, and total ROS formation was quantified using fluorescence microscopy as described in "Materials and Methods." Values are mean ± S.E.M of three independent experiments and ROS generation expressed as % of control. *significantly different from cells exposed to normoxia without NAC ($p < 0.05$); **significantly different from cells exposed to hyperoxia without NAC ($p < 0.01$). (For interpretation of the references to color in this figure legend, the reader is referred to the web version of this article at www.liebertonline.com/ars).

derived ROS may alter the interactions between blood cells and cells of the vessel wall to mediate cerebral microvascular dysfunction in sickle cell transgenic mice (42). Expression of Nox4 and other members of the Nox family are modulated in response to vascular injury and agents that induce damage to the vessel wall. Upregulation of Nox1 in arterial smooth muscle cells and an increase in Nox2 level in cells of adventitial origin during restenosis after carotid injury were observed as an early event that was followed by increased expression of Nox4 in smooth muscle cells (35). Similarly, differences in the relative expression of Nox2 and Nox4 in saphenous veins and arteries from patients undergoing coronary bypass surgery has been reported (13); however, the relative contributions of Nox4 and Nox2 to ROS production was not directly addressed. In HPAECs, blocking Nox2 with Nox2 siRNA blocked ~70% of hyperoxia-induced ROS/$O_2^{\cdot -}$ production as measured by DCFDA/hydroethidine oxidation, respectively (37). Similar to Nox2 siRNA, in the present study, knockdown of Nox4 with Nox4 siRNA only partially blocked hyperoxia-induced ROS/$O_2^{\cdot -}$ accumulation. Thus, in HPAECs, these combined results demonstrate the involvement of *both* Nox4 and Nox2 in hyperoxia-induced ROS generation. Interestingly, simultaneous knockdown of Nox2 and Nox4 with siRNA affected cell morphology, and induced cell death, suggesting a role for basal ROS generated via Nox2 and Nox4 in maintaining EC morphology and function. However, it is unclear if apoptosis or necrosis or both are involved in this process (S. Pendyala and V. Natarajan, results not shown).

Although the relative protein expression of both Nox4 and Nox2 in HPAECs was very similar under normoxia as compared to the mRNA expression (Table 1 and Fig. 2); exposure of cells to hyperoxia for 3 h increased mRNA and protein expression of Nox4, but not Nox2, which was concomitant to enhanced ROS generation. However, longer exposure to hyperoxia (24 h) stimulated Nox2 protein expression. This differential upregulation of Nox4 and Nox2 by hyperoxia at 3 h suggests that Nox4 could function as an

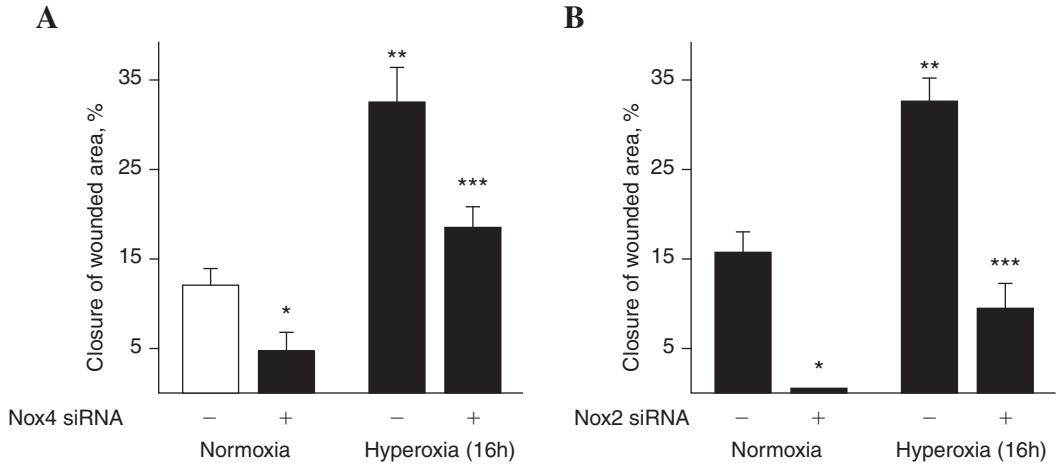

FIG. 11. Nox4 and Nox2siRNA attenuates hyperoxia-mediated cell migration. (**A** and **B**) HPAECs grown on 35-mm dishes to ~50% confluence were transfected with scrambled siRNA or Nox4 siRNA or Nox2 siRNA for 48 h. Cells were wounded as described in "Materials and Methods" and Fig. 10, and exposed to either normoxia or hyperoxia for 16 h. Values are mean ± S.E.M of three independent experiments in triplicates. *significantly different from scrambled siRNA transfected cells under normoxia ($p < 0.05$); *significantly different from scrambled siRNA transfected cells under normoxia ($p < 0.01$); ***significantly different from scrambled siRNA transfected cells under hyperoxia ($p < 0.001$).

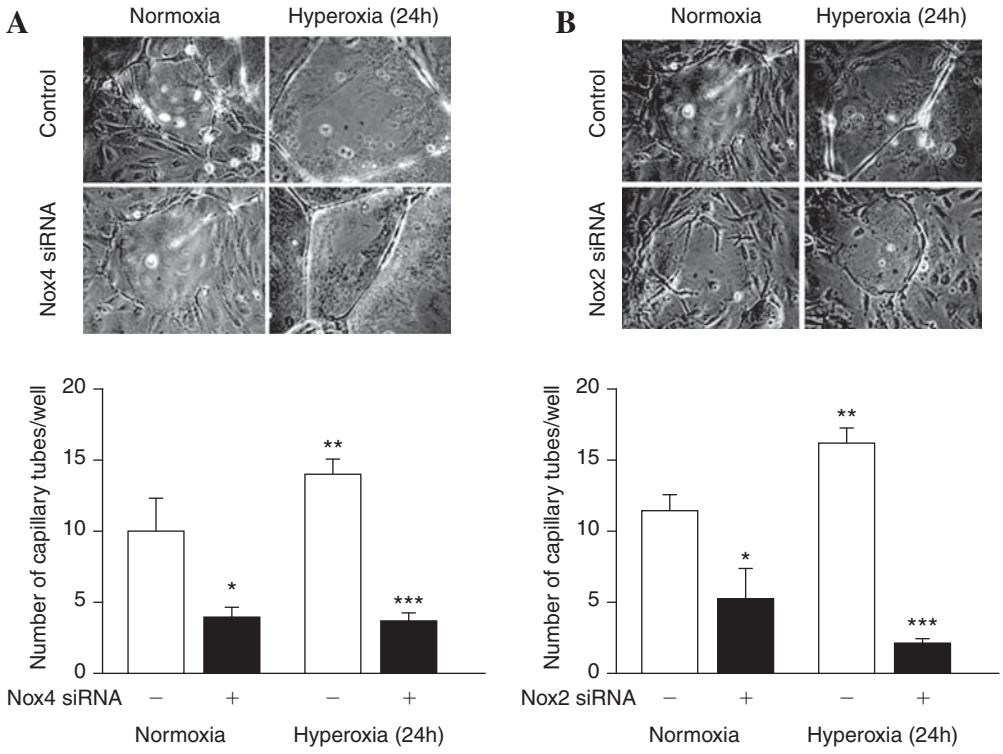

FIG. 12. Nox4 and Nox2 siRNA attenuates hyperoxia-mediated capillary tube formation. (**A** and **B**) HPAECs grown in 100-mm dishes to ~50% confluence were transfected with scrambled siRNA or Nox4 siRNA or Nox2 siRNA for 48 h. After 48 h, cells were trypsinized and seeded onto matrigel-coated 35-mm dishes, as described in "Materials and Methods." After 24 h of seeding, cells were either exposed to normoxia or hyperoxia (24 h) and formation of capillary tubes were visualized under phase-contrast microscope and quantified by counting different areas. Values are mean ± S.E.M of three independent experiments. *significantly different from scrambled siRNA transfected cells under normoxia ($p < 0.05$); **significantly different from scrambled siRNA transfected cells under normoxia ($p < 0.01$); ***significantly different from scrambled siRNA transfected cells under hyperoxia ($p < 0.00$).

oxygen sensor in the human pulmonary endothelium, which is physiologically at very low oxygen tension, and exposing them to higher oxygen levels (~95%) may trigger induction of the Nox4 isoform. Recent studies in distal tubular cells of the kidney also indicate that Nox4 could function as an oxygen sensor (22). Further studies are necessary to clarify the role of Nox4 as an oxygen sensor in hyperoxia.

Another interesting and novel observation in the present study was the nuclear localization of Nox4 and $p22^{phox}$ and redistribution of Nox4 from the nucleus to the cytosol after exposure of cells to hyperoxia. This was based on the distribution of native Nox4 in isolated nuclear fraction by immunofluorescence microscopy and Western blot analysis for Nox4 as well as the ability of Nox4 siRNA to knockdown Nox4 expression in nuclei. However, there are conflicting reports on the subcellular localization of Nox4 in nonphagocytic cells. In smooth muscle cells, Nox4 colocalizes with vinculin in focal adhesions and cell fractionation suggests nuclear localization of Nox4 (15), while in human aortic smooth muscle cells, Nox4 was localized in endoplasmic reticulum (16, 28). In HUVECs, native Nox4 was mainly nuclear; however, microinjection of Nox4-GFP fusion protein largely localized to endoplasmic reticulum (39), suggesting the possibility that the GFP tag may alter the localization of Nox4 protein. Thus, there are major differences in the cellular localization of native Nox4 *versus* overexpressed Nox4 for a given cell type. Although native Nox4 seems to have a predominant nuclear localization (32), the physiological significance of this nuclear localization of Nox4 is unclear. From our studies, we show that nuclear Nox4 is involved in the generation of hyperoxia-induced $ROS/O_2^{\cdot -}$ (Fig 6A). There is one report showing that Nox4 activity is independent of regulatory subunits in cell-free preparations from a tet-inducible system that allowed controlled Nox4 expression (17). This is consistent with earlier studies which showed that, while Nox4 requires $p22^{phox}$, mutation of the $p22^{phox}$ proline-rich domain (which serves as a docking site for other regulatory subunits) did not affect the activity of Nox4 (17). Further, a recent study shows that the nuclear fraction from HUVECs exhibits an NADPH-dependent $O_2^{\cdot -}$ producing activity supporting the role of Nox4 in generating ROS in the nucleus, where Nox4 likely forms a functional complex with $p22^{phox}$ (20). During analyses of Nox4, we did not detect any $p47^{phox}$ or Nox2 in the nuclear fractions; however, presence of $p22^{phox}$ was detected in the nuclear fraction by Western blot analysis and immunofluorescence microscopy. Furthermore, immuno-colocalization studies support an association between Nox4 and $p22^{phox}$ within the nucleus after 24 h exposure of cells to hyperoxia (Fig. 3A).

Accumulating evidence suggests that Nox enzymes are important sources of ROS in vascular tissues and cells, and enhanced production has been linked to the pathophysiology of several vascular/pulmonary disorders. In this context, our present results are novel, demonstrating existence of a compensatory mechanism in the endothelium for basal ROS generation in nanomolar range. We have shown that knockdown of Nox4 or Nox2 with siRNA upregulates the mRNA and protein expression of the other Nox homologue in HPAECs. A similar compensation of Nox4 mRNA was observed in $Nox2^{-/-}$ mice. Although $Nox2^{-/-}$ mice developed less lung injury, compared to control mice after exposure to hyperoxia for 48 and 72 h, our results show that deletion of Nox2 gene did not abrogate hyperoxia-induced lung injury suggesting potential roles of other Nox family members, such as Nox4, in ROS generation and lung injury. Silencing Nox4 with Nox4 siRNA increases Nox2 protein expression after 24 h of hyperoxia in HPAECs; therefore, conditional deletion of Nox4 or Nox2 or both in the lung will specifically address the role of these two Nox homologues in ROS generation in lung under normal and pathophysiological conditions.

The present work also provides evidence for the first time of Nox4-derived ROS in hyperoxia-induced EC motility and capillary tube formation. A similar role for Nox2-derived ROS in EC migration was observed in HPAECs as well as in HUVECs, suggesting a pivotal role of Nox-derived ROS in angiogenesis (38). Although, downregulation of Nox2 or Nox4 with siRNA upregulated protein expression of Nox4 or Nox2, respectively, the total ROS produced under hyperoxia was partially reduced compared to normoxia, indicating that the compensated protein may not be totally functional or may have a different spatial organization. Similarly, with wound closure or capillary tube formation after exposure to hyperoxia, a complete compensation of the function with Nox2 or Nox4 siRNA was not observed (Figs. 11 and 12). These results also suggest that the expression of both Nox4 and Nox2 are critical for optimal ROS production, wound closure, and tube formation in response to hyperoxia. Additionally, Nox4 and Nox2 proteins may have signaling function(s), independent of ROS generation, in cell motility and angiogenesis, which warrants further investigation. In human airway smooth muscle cells, Nox4 mediates TGF-β1-induced phosphorylation of retinoblastoma protein, proliferation, and hypertrophy, which are redox-dependent (33). Although ROS-derived from Nox4 or Nox2 could account for many of the signaling cascades and functions in vascular cells, Nox4 may have a role in oxygen sensing in the kidney cortex (11), and to regulate TASK-1 activity (22). Further more, an increasing number of studies point to Nox-derived ROS being anti-apoptotic in pancreatic cancer cells (40), while Nox1 regulates apoptosis and potentially stimulates branching morphogenesis in sinusoidal endothelial cells (18)

In summary, our study demonstrates a role for Nox4 and Nox2 in hyperoxia-induced $ROS/O_2^{\cdot -}$ production in an *in vitro* model of human lung ECs and in an *in vivo* $Nox2^{-/-}$ murine model. Our results show that Nox4 mRNA and protein expression are upregulated by hyperoxia and the involvement of Nox4 as well as Nox2 in hyperoxia-induced $ROS/O_2^{\cdot -}$ production in HPAECs. We also demonstrate that hyperoxia-induced cell migration and capillary tube formation are regulated by ROS generated via a Nox4-dependent pathway. In $Nox2^{-/-}$ mice, we demonstrate higher basal expression of Nox4 mRNA compared to control mice, suggesting the induction of a compensatory mechanism for Nox-dependent ROS generation. While the exact mechanism of hyperoxia-induced upregulation of Nox4 expression in HPAECs and mouse lung from $Nox2^{-/-}$ mice is yet to be defined, our studies indicate a potential role for Nrf2 in hyperoxia-induced Nox4 expression (29). Further studies are in progress to unravel the role of Nrf2 and related signaling pathways activated by hyperoxia in regulating Nox4 expression and $ROS/O_2^{\cdot -}$ production in vascular endothelium.

Acknowledgments

The authors would like to thank Thomas Leto from NIH for providing Nox4 wt plasmid. This work was supported by National Heart, Lung and Blood Institute Grant HL 08553 to V.N.

Abbreviations

CT, threshold cycle; DAPI, 4, 6-diamidino-2-phenylindol; DCF, 2, 7-dichlorofluorescein; DCFH-DA, 2, 7-dichlorofluorescin diacetate; ECL, enhanced chemiluminescence; EDTA, ethylenediaminetetraacetate; MAPK, mitogen-activated protein kinase; ROS, reactive oxygen species; siRNA, small interfering RNA.

Disclosure Statement

No competing financial interest exist.

References

1. Babior BM. The leukocyte NADPH oxidase. *Isr Med Assoc J* 11: 1023–1024, 2002.
2. Babior BM. NADPH oxidase: An update. *Blood* 93: 1464–1476, 1999.
3. Bokoch GM and Knaus UG. NADPH oxidases: Not just for leukocytes anymore. *Trends Biochem Sci* 28: 502-508, 2003.
4. Brueckl C, Kaestle S, Kerem A, Habazettl H, Krombach F, Kuppe H, and Kuebler WM. Hyperoxia-induced reactive oxygen species formation in pulmonary capillary endothelial cells *in situ*. *Am J Respir Cell Mol Biol* 34: 453–463, 2006.
5. Cai H. Hydrogen peroxide regulation of endothelial function: Origins, mechanisms, and consequences. *Cardiosvasc Res* 68: 26–36, 2005.
6. Cai H, Griendling KK, and Harrison DG. The vascular NAD(P)H oxidases as therapeutic targets in cardiovascular diseases. *Trends Pharmacol Sci* 24: 471–478, 2003.
7. Chowdhury AK, Watkins T, Parinandi NL, Saatian B, Kleinberg ME, Usatyuk PV, and Natarajan V. Src-mediated tyrosine phosphorylation of p47phox in hyperoxia-induced activation of NADPH oxidase and generation of reactive oxygen species in lung endothelial cells. *J Biol Chem* 280: 20700–20711, 2005.
8. Decoursey TE and Ligeti E. Regulation and termination of NADPH oxidase activity. *Cell Mol Life Sci* 62: 2173–2193, 2005.
9. Djordjevic T, BelAiba RS, Bonello S, Pfeilschifter J, Hess J, and Görlach A. Human urotensin II is a novel activator of NADPH oxidase in human pulmonary artery smooth muscle cells. *Arterioscler Thromb Vasc Biol* 25: 519–525, 2005.
10. Etoh T, Inoguchi T, Kakimoto M, Sonoda N, Kobayashi K, Kuroda J, Sumimoto H, and Nawata H. Increased expression of NAD(P)H oxidase subunits, NOX4 and p22phox, in the kidney of streptozotocin-induced diabetic rats and its reversibility by interventive insulin treatment. *Diabetologia* 46: 1428–1437, 2003.
11. Geiszt M and Leto TL. The Nox family of NAD(P)H oxidases: host defense and beyond. *J Biol Chem* 279: 51715–51718, 2004.
12. Ghaemmaghami S, Huh WK, Bower K, Howson RW, Belle A, Dephoure N, O'Shea EK, and Weissman IS. Global analysis of protein expression in yeast. *Nature* 425: 738–741, 2003.
13. Guzik TJ, Sadowski J, Kapelak B, Jopek A, Rudzinski P, Pillai R, Korbut R, and Channon KM. Systemic regulation of vascular NAD(P)H oxidase activity and nox isoform expression in human arteries and veins. *Arterioscler Thromb Vasc Biol* 9: 1614–1620, 2004.
14. Gygi SP, Rochon Y, Franza BR, and Aebersold R. Correlation between protein and mRNA abundance in yeast. *Molec Cell Biol* 3: 1720–1730, 1999.
15. Hilenski LL, Clempus RE, Quinn MT, Lambeth JD, and Griendling KK. Distinct subcellular localizations of Nox1 and Nox4 in vascular smooth muscle cells. *Arterioscler Thromb Vasc Biol* 24: 677–683, 2004.
16. Kalinina N, Agrotis A, Tararak E, Antropova Y, Kanellakis P, Ilyinskaya O, Quinn MT, Smirnov V, and Bobik A. Cytochrome b558-dependent NAD(P)H oxidase-phox units in smooth muscle and macrophages of atherosclerotic lesions. *Arterioscler Thromb Vasc Biol* 22: 2037–2043, 2002.
17. Kawahara T, Ritsick D, Cheng G, and Lambeth JD. Point mutations in the proline-rich region of p22phox are dominant inhibitors of Nox1- and Nox2-dependent reactive oxygen generation. *J Biol Chem* 280: 31859–31669, 2005.
18. Kobayashi S, Nojima Y, Shibuya M, and Maru Y. Nox1 regulates apoptosis and potentially stimulates branching morphogenesis in sinusoidal endothelial cells. *Exp Cell Res* 300: 455–462, 2004.
19. Krause KH. Tissue distribution and putative physiological function of NOX family NADPH oxidases. *Jpn J Infect Dis* 57: S28–S29, 2004.
20. Kuroda J, Nakagawa K, Yamasaki T, Nakamura K, Takeya R, Kuribayashi F, Imajoh–Ohmi S, Igarashi K, Shibata Y, Sueishi K, and Sumimoto H. The superoxide-producing NAD(P)H oxidase Nox4 in the nucleus of human vascular endothelial cells. *Genes Cells* 10: 1139–1151, 2005.
21. Landmesser U, Cai H, Dikalov S, McCann L, Hwang J, Jo H, Holland SM, and Harrison DG. Role of p47(phox) in vascular oxidative stress and hypertension caused by angiotensin II. *Hypertension* 40: 511–515, 2002.
22. Lee YM, Kim BJ, Chun YS, So I, Choi H, Kim MS and Park JW. NOX4 as an oxygen sensor to regulate TASK-1 activity. *Cell Signal* 18: 499–507, 2006.
23. Li JM and Shah AM. Intracellular localization and preassembly of the NADPH oxidase complex in cultured endothelial cells. *J Biol Chem* 277: 19952–19960, 2002.
24. Li JM and Shah AM. Endothelial cell superoxide generation: regulation and relevance for cardiovascular pathophysiology. *Am J Physiol Regul Integr Comp Physiol* 287: R1014–R1030, 2004.
25. Mahadev K, Motoshima H, Wu X, Ruddy JM, Arnold RS, Cheng G, Lambeth JD, and Goldstein BJ. The NAD(P)H oxidase homolog Nox4 modulates insulin-stimulated generation of H2O2 and plays an integral role in insulin signal transduction. *Mol Cell Biol* 24: 1844–1854, 2004.
26. Nagata K, Iwasaki Y, Yamada T, Yuba T, Kono K, Hosogi S, Ohsugi S, Kuwahara H, and Marunaka Y. Overexpression of manganese superoxide dismutase by N-acetylcysteine in hyperoxic lung injury. *Respir Med* 101: 800–807, 2007.
27. Parinandi NL, Kleinberg MA, Usatyuk PV, Cummings RJ, Pennathur A, Cardounel AJ, Zweier JL, Garcia JG, and Natarajan V. Hyperoxia-induced NAD(P)H oxidase activation and regulation by MAP kinases in human lung endothelial cells. *Am J Physiol Lung Cell Mol Physiol* 284: L24–L25, 2003.
28. Pedruzzi E, Guichard C, Ollivier, Driss F, Fay M, Prunet C, Marie JC, Pouzet C, Samadi M, Elbim C, O'dowd Y, Bens M, Vandewalle A, Gougerot–Pocidalo MA, Lizard G, and Ogier–Denis E. NAD(P)H oxidase Nox-4 mediates

7-ketocholesterol-induced endoplasmic reticulum stress and apoptosis in human aortic smooth muscle cells. *Mol Cell Biol* 24: 10703–10717, 2004.
29. Pendyala S, Gorshkova IA, He DH, Cho HY, Kleeberger SR, and Natarajan V. Nrf2 regulates hyperoxia-mediated Nox4 expression and ROS production. *Am J Resp Crit Care Med* Abstract 175, 2007.
30. San Martin A, Foncea R, Laurindo FR, Ebensperger R, Griendling KK, and Leighton F. Nox1-based NADPH oxidase-derived superoxide is required for VSMC activation by advanced glycation end-products. *Free Radic Biol Med* 42: 1671–1679, 2007.
31. Schreibelt G, Kooij G, Reijerkerk A, van Doorn R, Gringhuis SI, van der Pol S, Weksler BB, Romero IA, Couraud PO, Piontek J, Blasig IE, Dijkstra CD, Ronken E, and de Vries HE. Reactive oxygen species alter brain endothelial tight junction dynamics via RhoA, PI3 kinase, and PKB signaling. *FASEB J* 21: 3666–3676, 2007.
32. Shiose A, Kuroda J, Tsuruya K, Hirai M, Hirakata H, Naito S, Hattori M, Sakaki Y, and Sumimoto H. A novel superoxide-producing NAD(P)H oxidase in kidney. *J Biol Chem* 276: 1417–1423, 2001.
33. Sturrock A, Huecksteadt TP, Norman K, Sanders, K, Murphy TM, Chitano P, Wilson K, Hoidal JR, and Kennedy TP. Nox4 mediates TGF-beta1-induced retinoblastoma protein phosphorylation, proliferation, and hypertrophy in human airway smooth muscle cells. *Am J Physiol Lung Cell Mol Physiol* 292: L1543–L1555, 2007.
34. Sumimoto H, Miyano K, and Takeya R. Molecular composition and regulation of the Nox family NAD(P)H oxidases. *Biochem Biophys Res Commun* 338: 677–686, 2005.
35. Szöcs K, Lassègue B, Sorescu D, Hilenski LL, Valppu L, Couse TL, Wilcox JN, Quinn MT, Lambeth JD, and Griendling KK. Upregulation of Nox-based NAD(P)H oxidases in restenosis after carotid injury. *Arterioscler Thromb Vasc Biol* 22: 21–27, 2002.
36. Thannickal VJ and Fanburg BL. Reactive oxygen species in cell signaling. *Am J Physiol Lung Cell Mol Physiol* 279: L1005–L1028, 2000.
37. Usatyuk PV, Romer LH, He D, Parinandi NL, Kleinberg ME, Zhan S, Jacobson JR, Dudek SM, Pendyala S, Garcia JG, and Natarajan V. Regulation of hyperoxia-induced NADPH oxidase activation in human lung endothelial cells by the actin cytoskeleton and cortactin. *J Biol Chem* 282: 23284–23295, 2007.
38. Ushio–Fukai M. Redox signaling in angiogenesis: role of NADPH oxidase. *Cardiovasc Res* 71: 226–235, 2006.
39. Van Buul JD, Fernandez–Borja M, Anthony EC, and Hordijk PL. Expression and localization of NOX2 and NOX4 in primary human endothelial cells. *Antioxid Redox Signal* 7: 308–317, 2005.
40. Vaquero EC, Edderkaoui M, Pandol SJ, Gukovsky I, and Gukovskaya AS. Reactive oxygen species produced by NAD(P)H oxidase inhibit apoptosis in pancreatic cancer cells. *J Biol Chem* 279: 34643–34654, 2004.
41. Wolin MS. Subcellular localization of Nox-containing oxidases provides unique insight into their role in vascular oxidant signaling. *Arterioscler Thromb Vasc Biol* 24: 625–627, 2004.
42. Wood KC, Hebbel RP, and Granger DN. Endothelial cell NADPH oxidase mediates the cerebral microvascular dysfunction in sickle cell transgenic mice. *FASEB J* 19: 989–991, 2005.

Address reprint requests to:
Viswanathan Natarajan, Ph.D.
Section of Pulmonary
and Critical Care
Department of Medicine
The University of Chicago
Chicago, IL 60637.

E-mail: vnataraj@medicine.bsd.uchicago.edu

Date of first submission to ARS Central, July 22, 2008; date of final revised submission, September 10, 2008; date of acceptance, September 10, 2008.